A new methodology for performing large scale simulations of tsunami generated by deformable submarine slides

Rebecca C. Smith[a,1,*], Jon Hill[b], Simon L. Mouradian[a], Matthew D. Piggott[a], Gareth S. Collins[a]

[a] *Department of Earth Science and Engineering, Imperial College London, SW7 2AZ, UK.*
[b] *Department of Geography and Environment, University of York, Heslington, York, YO10 5DD, UK*

Abstract

Large tsunamis can be generated by submarine slides, but these events are rare on human timescales and challenging to observe. Experiments and numerical modelling offer methods to understand the mechanisms by which they generate waves and what the potential hazard might be. However, to fully capture the complex waveform generated by a submarine slide, the slide dynamics must also be accurately modelled. It is computationally difficult to model both a three-dimensional submarine slide whilst simultaneously simulating oceanic-scale tsunamis. Past studies have either coupled localised models of the slide generation to oceanic-scale tsunami simulations or simplified the slide dynamics. Here, we present a new methodology of model coupling that generates the wave in the ocean-scale model via boundary-condition coupling of a two-dimensional dynamic slide simulation. We verify our coupling methodology by comparing model results to a previous simulation of a tsunamigenic slide in the Gulf of Mexico. We then examine the effect of slide deformation on the risk posed by hypothetical submarine slides around the UK. We show the deformable

*Corresponding author
Email address: `rebecca.smith08@alumni.imperial.ac.uk` (Rebecca C. Smith)

[1] Present Address: Risk Management Solutions, 30 Monument Street, London, EC3R 8NB, UK

submarine slide simulations produce larger waves than the solid slide simulations due to the details of acceleration and velocity of the slide, although lateral spreading is not modelled. This work offers a new methodology for simulating oceanic-scale tsunamis caused by submarine slides using the output of a two–dimensional, multi-material simulation as input into a three–dimensional ocean model. This facilitates future exploration of the tsunami risk posed by tsunamigenic submarine slides that affect coastlines not normally prone to tsunamis.

Keywords:
Submarine Slide, Tsunami, Numerical Modelling, Landslides,

1. Introduction

Tsunamigenic submarine slides are rare on human timescales and are difficult to monitor or directly observe because it is not possible to predict their occurrence. Therefore, experiments and numerical modelling are important for understanding the submarine slide dynamics, failure, tsunamigenic potential, and forecasting the characteristics of the generated tsunami (Masson et al., 2006; Harbitz et al., 2014). Laboratory experiments are useful to approximate natural conditions with typical materials, however numerical modelling is the only way to simulate events at real scale and with complete and complex geometry and bathymetry (Bornhold and Thomson, 2012). This is essential to assess the potential hazard posed by such events.

The passive Atlantic margin is the source of a number of geologically recent submarine slides, the largest of which was the Storegga Slide, which occurred offshore Norway approximately 8.2 ka (Bugge et al., 1988; Dawson et al., 1988; Smith et al., 2004; Bondevik et al., 2005a; Wagner et al., 2007) with an estimated slide volume of 2400–3200 km^3 (De Blasio et al., 2005). Deposits from the resulting tsunami indicate vertical run–ups of over 20 m on the Shetlands Islands and Norwegian coast

(Bondevik et al., 2005a,b; Dawson et al., 1988; Smith et al., 2004; Wagner et al., 2007). Storegga is the most recent of a series of large submarine slides that have occurred in this area of the Nordic Seas throughout geological history (Laberg et al., 2002a,b; Bryn et al., 2003; Solheim et al., 2005). There is some debate over the recurrence interval, however, the most recent studies suggest six very large slides occurred in the last 20 ka, which indicates a recurrence interval of 3–4 ka for the area (Talling, 2013). Furthermore, not all slides on the Norwegian and UK margins may have also initiated tsunami, depending on the size, depth, speed and acceleration of slide blocks.

Studies of submarine slide tsunami often break the process down into four parts: 1) the dynamics of the submarine slide, 2) the wave generation, 3) the wave propagation and 4) the tsunami wave inundation/run-up at coastlines. Numerical modelling of large–scale submarine slide generated tsunami from the initiation of submarine slide motion and wave generation, through to wave propagation and inundation in three dimensions, is computationally challenging, owing to the large slide dimensions and long run-out distances. Furthermore, within the large computational domains required, many aspects must be modelled at high resolution, such as the slide motion and the coastlines. Therefore, numerical simulations have tended to rely on simplifications to make the problem more tractable.

Many studies have simplified steps (1)–(3) by modelling the slide as a rigid block with prescribed motion, and employing the shallow–water approximation (e.g. Harbitz 1992; Ma et al. 2012 and Hill et al. 2014). However, rigid block models do not account for deformation of the slide and incorporate profiles for slide velocity and acceleration that must be estimated. Since several studies have shown that submarine slide acceleration and velocity are key parameters in determining resulting wave characteristics (Harbitz, 1992; Harbitz et al., 2014; Løvholt et al., 2015), this suggests that accurate representation of the slide dynamics is imperative to achieve accurate wave heights in simulations. The shallow water (long–wave) approximation relies on the assumption that the horizontal scale of the wave motion is considerably larger than the local water depth or vertical scale (Harbitz, 1992; Jiang and LeBlond, 1992, 1993; Thomson et al., 2001; Fine et al., 1998, 2005; Assier-Radkiewicz et al., 2000; Yavari-Ramshe and Ataie-Ashtiani, 2015). Shallow water models become increasingly less appropriate in increasing water depths and decreasing water wavelengths, as dispersion becomes more important (Bornhold and Thomson, 2012) and this approximation neglects frequency dispersion and vertical velocity/acceleration. Whilst this approximation is generally appropriate for seismogenic tsunami, it may not be appropriate for submarine slide generated waves, which often have shorter wavelengths (Glimsdal et al., 2013; Løvholt et al., 2015).

Some numerical studies have modelled deformation of submarine slides. In order to model the slide deformation, many of these studies are restricted in terms of domain size, scale or consider an approximation to the full Navier–Stokes equations. Studies that model the slide as a Newtonian, viscous fluid but were restricted to lab scale are Assier-Rzadkiewicz et al. (1997) and Abadie et al. (2010). Fine et al. (2005) and Assier-Radkiewicz et al. (2000) employ similar slide models but rely on the shallow water approximation in order to model a full–scale slide. Some studies have also used a Bingham rheology for the slide, a non-Newtonian fluid where the deformation is dependant on stress. Examples of this at the laboratory scale include Assier-Rzadkiewicz et al. (1997) and Gauer et al. (2005). Jiang and LeBlond (1993) and Gauer et al. (2006) use a similar rheological model over a large domain, but applying the shallow water approximation. Ma et al. (2013) modelled the slides as a water–sediment mixture and Capone et al. (2010), Ataie-Ashtiani and Shobeyri (2008) and Snelling et al. (2020) used Smoothed Particle Hydrodynamics (SPH) to recreate laboratory experiments. Lee and Huang (2018) and Yu and Lee (2019) used a multi–phase flow model to simulate underwater landslides and wave generation. Many of the domains considered in these studies are restricted to a small area due to the high-resolution required to capture the dynamics of the slide. In order to simulate the tsunami propagation a second model has to be coupled to the slide model or the spatial resolution is too low to capture detailed dynamics in the waveform generated by the slide motion.

In reality, submarine slides deform with complex rheology and flow (Grilli and Watts, 2005; Løvholt et al., 2015). Simulating the slide dynamically, including its interaction with the water, internal deformation and drag, ensures a more accurate description of slide acceleration and velocity, but adds substantial complexity and computational expense. The importance of realistic slide dynamics (i.e. acceleration and maximum velocity) and internal deformation during the wave-generating stage of slide motion motivates the choices of numerical modelling approach used in this work. While approximations to the full Navier-Stokes equations are often valid, in order to investigate fully the effects and importance of slide dynamics and deformability on wave generation, the use of full Navier-Stokes models allows vertical acceleration to be considered and provides a more complete representation than shallow water models, particularly for relatively small slides (Watts et al., 2003; Abadie et al., 2012; Glimsdal et al., 2013; Horrillo et al., 2013).

Fluidity is a computational fluid dynamics framework that allows for the numerical solution of several equation sets in three dimensions (Piggott et al., 2008; AMCG, 2014). Fluidity has previously been used in two dimensions to model deformable submarine slides and accurately represent slide, water (and air) to simulate the generation of tsunami waves (Smith et al., 2016). The approaches in Smith et al. (2016) explicitly modelled the submarine slides (as Newtonian viscous fluids) and therefore helped to improve understanding of the submarine slide failure process and the forces that act upon the slide and water. However, the methods are computationally expensive to run owing to the modelling of multiple materials and requirement of high resolution meshes to resolve the complex and small-scale slide dynamics and the coupling to wave generation. The application of mesh adaptivity was able to reduce the computational expense, but the ability to apply this to much larger, and three-dimensional, computational domains is still restricted. Therefore previous work only considered two-dimensional, vertical slice domains over the tsunami generation region (Smith et al., 2016). To fully quantify the importance of slide deformation and dynamics for a hazard assessment, it is important to study wave generation and propagation in three dimensions to allow consideration of geometric spreading, wave interaction with the coastlines, the effect of the direction of slide failure and wave inundation. Extending multi-material approaches to significantly larger domains, whilst maintaining the high resolution and number of materials would require an increase in computational cost that is not currently practical. Therefore other approaches that are less computationally demanding are required.

A new, computationally efficient approach for modelling submarine slide tsunami is presented here that accounts for slide dynamics and deformation, and wave generation and propagation, in three dimensions using Fluidity (Piggott et al., 2008). The motion of the submarine slide is incorporated via a prescribed boundary condition applied on the sea floor of the computational domain (e.g. Hill et al. 2014). This mimics the effect of the submarine slide motion on the water column and allows the number of materials that are modelled to be reduced by omitting the submarine slide and modelling only the water. Consequently, the requirement for high vertical resolution is removed and thus computational expense is reduced significantly. As a result, the model can be applied over an increased area, and in three dimensions, to model the generation and propagation of the wave towards coastlines. This approach is referred to as the Single Material (SM) method. Previously, such approaches have assumed a rigid slide body (that cannot fully account for all the forces acting upon a submarine slide that will in turn affect wave generation) and a simplified, idealised acceleration and deceleration profile. This approach is similar to that used by Fine et al. (2005), Ma et al. (2012) and Harbitz (1992) but is novel in that the full Navier-Stokes equations are used instead of the shallow water approximation, and differs from Harbitz (1992) where the free surface height is altered in the shallow water equations. We use three different numerical approaches to model submarine slide tsunami, within the same framework. This has allowed for comparison of approaches without the complication of separate models and an understanding of the limitations and advantages of each method. These three-dimensional modelling techniques are then applied to advance understanding of the coastal hazard from submarine slide tsunami.

1.1. Outline

In this work, the output (change in position and thickness of a slide) of a two–material simulation (MM2FS, Smith et al. 2016), is extracted and used as a boundary condition for the single-material (SM) simulation. The coupling of these models forms an approach termed Single Material, Deformable Slide, Simulated Velocity (SM-DS-SV). Another approach uses a rigid slide with a velocity profile (SM-RS-EV: Single Material, Rigid Slide, Estimated Velocity) that is estimated using a simple momentum balance on an inclined slope that is representative of the slope on which the slides lies (Harbitz, 1992). A further approach assigns a velocity profile to the rigid slide that is based on the motion of the centre of mass of the slide in an MM2FS simulation. This is a 'hybrid' approach between a rigid slide with a synthetic, estimated velocity profile (SM-RS-EV) and a simulation that attempts to account for more realistic slide dynamics and deformation using information extracted from simulations that model the slide as a fluid. This approach is termed Single Material, Rigid Slide, Simulated Velocity (SM-RS-SV). By comparing the waves generated by the SM-RS-SV approach with the SM-DS-SV approach, the effect and importance of slide deformation for wave generation can be isolated from the importance of slide velocity and acceleration. Waves produced by these three methods are also compared to waves produced by a rigid slide of equal volume moving with a prescribed velocity profile, using a method similar to Harbitz (1992); Ma et al. (2012); Hill et al. (2014).

These approaches are first applied to a hypothetical submarine slide scenario in the Gulf of Mexico (first modelled in two and three dimensions in Horrillo et al. (2013) and in two dimensions in Smith et al. (2016)) and is now extended to three dimensions using Fluidity and the SM-RS-EV, SM-RS-SV and SM-DS-SV approaches to verify correct implementation of the model. We then show the effect modelling deformation of the tsunamigenic slide has on tsunami risk from two hypothetical slides offshore of the UK.

2. Methods

2.1. Fluidity

Fluidity is an open source, general purpose, computational fluid dynamics, framework (Piggott et al., 2008). The flexible finite-element/control-volume discretisation approach, allows for the numerical solution of several equation sets (Piggott et al., 2008). It has been used in a number of fluid flow studies, ranging from laboratory to ocean-scale (e.g. Wells et al., 2010; Hill et al., 2012; Hiester et al., 2011; Parkinson et al., 2014). In an ocean modelling context, Fluidity has been used to model both modern and ancient earthquake-generated tsunami (Oishi et al., 2013; Mitchell et al., 2010; Shaw et al., 2008), and tsunami generated by three-dimensional rigid-block submarine slides with prescribed motion, in a study of the ancient Storegga Slide (Hill et al., 2014). Fluidity uses unstructured meshes, which can be multiscale but fixed, or fully dynamically adaptive. Multiscale meshes have spatially varying resolution, which can vary by orders of magnitude (Piggott et al., 2008). This enables complex coastlines and bathymetry to be accurately represented without "staircase" effects (Wells et al., 2005). The reduction in computational expense by using multiscale or adaptive meshes may allow for the simulation of wave generation and propagation of slides that are larger than it has previously been possible to model. Here, the non-hydrostatic incompressible Navier-Stokes equations under the Boussinesq approximation are solved in a rotating reference frame:

$$\frac{\partial \boldsymbol{u}}{\partial t} + \boldsymbol{u} \cdot \nabla \boldsymbol{u} + 2\boldsymbol{\Omega} \times \boldsymbol{u} = -\nabla \left(\frac{p}{\rho}\right) + \nabla \cdot (\boldsymbol{\nu} \nabla \boldsymbol{u}) - g\boldsymbol{k}, \tag{1a}$$

$$\nabla \cdot \boldsymbol{u} = 0, \tag{1b}$$

where $\boldsymbol{u}$ is the 3D velocity vector, t represents time, p is pressure, $\boldsymbol{\nu}$ is the kinematic viscosity tensor and ρ denotes the density, which is constant in this work. $\boldsymbol{\Omega}$ is the rotational velocity of the Earth and g is the gravitational acceleration with $\boldsymbol{k}$ pointing in the radial, upward direction. The seabed boundary condition is then dictated by the methodology used.

2.2. MM2FS: Two-material model: viscous slide and water, with a free surface

The MM2FS approach is one of a number of approaches for modelling submarine slide tsunami generation introduced in Smith et al. (2016). Two materials (slide and water) are modelled as viscous fluids and described using volume fraction fields with different densities and viscosities. The slide is simulated in two-dimensions along the vertical plane in which the slide travels.

For incompressible flows with variable density, as in the case of multiple materials, an additional equation is required to close the system, we refer to this as the equation of state. In the approach used here, this equation relates the bulk density to the volume fractions of materials in the problem, along with the associated material properties.

A volume fraction field, φ_i, is used to describe the location of different materials. In MM2FS $n_\varphi = 2$, φ_i varies in $[0, 1]$ and should sum to unity everywhere:

$$\sum_{i=1}^{n_\varphi} \varphi_i = 1. \tag{2}$$

Since, from (2), one of the volume fraction fields (here always water) can be recovered from the others using

$$\varphi_{n_\varphi} = 1 - \sum_{i=1}^{n_\varphi - 1} \varphi_i, \tag{3}$$

$n_\varphi - 1$ advection equations of the form

$$\frac{\partial \varphi_i}{\partial t} + \mathbf{u} \cdot \nabla \varphi_i = 0, \tag{4}$$

need to be solved for the landslide.

In MM2FS, only one volume fraction is required, therefore only the landslide is tracked using Equation (4), while the location of the water is recovered using Equation (3). The bulk density and viscosity used in Equation (1a) is recovered from the volume fractions using:

$$\rho = \sum_{i=1}^{n_\varphi} \varphi_i \rho_i, \qquad \mu = \sum_{i=1}^{n_\varphi} \varphi_i \mu_i, \tag{5}$$

where ρ_i and μ_i represent the constituent densities and viscosities of the individual materials. This method is similar to the VoF method used in TSUNAMI3D (Horrillo et al., 2013) and OpenFoam (Abadie et al., 2010). For more details of this model see Smith et al. (2016) and Smith (2017).

2.3. SM: Single material and prescribed velocity boundary condition

Submarine slide failure leads to water displacement. In this approach the total water displacement is determined by the change in slide thickness along the ocean floor caused by the slide movement. This water displacement is imposed as a normal velocity Dirichlet boundary condition on the ocean floor, inducing a change in the normal velocity, and is calculated as:

$$(\boldsymbol{u} \cdot \boldsymbol{n})^D = \frac{[h_s(x - x_s(t - \Delta t), y - y_s(t - \Delta t))] - [h_s(x - x_s(t), y - y_s(t))]]}{\Delta t} \quad (6)$$

where Δt is the timestep of the model, and $\boldsymbol{n}$ is the outward unit normal. The parameters x_s and y_s are the horizontal coordinates and h_s is slide thickness. The velocity vector is approximated using a linear discontinuous Galerkin approximation (P1DG), whilst a quadratic continuous (P2) approximation is used for pressure. Further details of the numerics may be found in Hill et al. (2014).

Fluidity is parallelised and this methodology is applied in all three single material approaches (SM–RS–EV, SM–RS–SV and SM–DS–SV) irrespective of a solid or deforming slide. Hill et al. (2014) tested Fluidity's SM–RS–EV approach against Haugen et al. (2005) in two dimensions and achieved good agreement between the two models for a rigid slide. Three approaches to model the slide dynamics are detailed below and summarised in Table 1.

2.3.1. SM-DS-SV approach: Single material, deformable slide, simulated velocity

The following work–flow is undertaken to move from two–dimensional multimaterial, multilayer simulations to three–dimensional, single material, single layer simulations:

1. Run two-dimensional MM2FS simulation.

2. Extract from MM2FS the geometry/thickness and position of the slide, as a function of distance, through time.
3. Use a low pass filter to smooth high-frequency fluctuations in the slide thickness profile
4. Calculate the change in thickness of the slide, h_s, for every column of nodes in the mesh. between the current timestep and the previous timestep to give a velocity ($dv = dh/dt$)
5. Apply this velocity as boundary condition at the sea floor, in the local normal direction, in a simulation with reduced vertical resolution. The velocity boundary condition is applied perpendicular to the slide transect, to a distance of half the width of the slide either side.

Step (3) is required to remove any effect of the mesh on the shape of the submarine slide by filtering out high-frequency fluctuations (discussed in Smith et al., 2016 and Horrillo et al., 2013). These fluctuations are caused by the sharp gradient in density and velocity at the slide surface. The parameters of the low pass filter were chosen so that the overall shape of the slide is preserved, but minor mesh-scale noise (occurring on scales $<$100 m, the horizontal resolution of the MM2FS simulation) in slide thickness is smoothed. This step ensures that when dh/dt is calculated the mesh-scale changes are smoothed out and are negligible compared to the long wavelength change in shape of the slide and does not result in ‘pulses’ in which could lead to a ‘noisy’ boundary condition. Furthermore, the resolution in the slide region of the SM–DS–SV simulation is coarser than the resolution in the MM2FS simulation and therefore high frequency noise at this scale could not be accurately reproduced on the coarser mesh.

2.3.2. SM-RS-SV approach: Single material, rigid slide, simulated velocity

1. Run two-dimensional MM2FS simulation.
2. Extract the displacement of the slide's centre of mass from the MM2FS simulation.
3. Calculate the velocity profile of the slide's centre of mass using the displacement extracted in (2) and the timestep.
4. Prescribe the motion of a rigid slide, with fixed and constant slide thickness using a choice of one of these two velocities.

2.3.3. SM-RS-EV approach: Single material, rigid slide, estimated velocity

To estimate a velocity profile for the submarine slides in this work, a force balance for a submerged submarine slide on a constant slope is used (Harbitz, 1992).

$$u_{term} = \sqrt{\frac{2(\rho_s - \rho_w)gh(\sin\alpha - \mu\cos\alpha)}{C_D\rho_w}}, \tag{7}$$

where ρ_s is the mean slide density, ρ_w is the density of the water surrounding the slide, h is the average slide thickness, α is the slope angle, μ the coefficient of friction between the slide and the seafloor, g the acceleration due to gravity and C_D is the drag coefficient along the upper surface of the slide. Applying Equation (7) to the Storegga Slide for reasonable values of μ and C_D, suggests $u_{term} = 56$ ms^{-1}, however studies show the maximum slide velocity that gives the best match to observed run-up heights was about 60% of this, 35 ms^{-1} (Bondevik et al., 2005b; Hill et al., 2014). Therefore the maximum velocity of the slides in this work is taken to be 60% of u_{term}. The values for μ (0.005) and C_D (0.0025) are fixed and taken from Hill et al. (2014). ρ_w and ρ_s are chosen to match the values in the MM2FS simulations (Smith et al., 2016), 1000 kgm^{-3} and 2000 kgm^{-3} respectively. Therefore u_{max} is solely a function

Table 1: Comparison of SM-RS-EV, SM-RS-SV and SM-DS-SV approaches

	Vertical Velocity/ Shape Change	**Horizontal Velocity/ Slide Velocity**
SM-RS-EV **Single Material,** **Rigid Slide,** **Estimated Velocity**	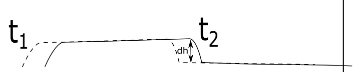 $v = \frac{dh}{dt} = \frac{(h_{t_1} - h_{t_2})}{(t_2 - t_1)}$ For every node in the mesh in MM2FS	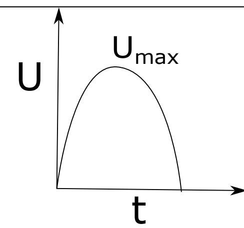
SM-RS-SV **Single Material,** **Rigid Slide,** **Simulated Velocity**	As above	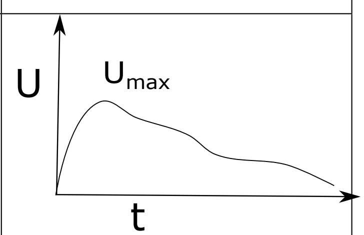 where the velocity is the centre of mass of the slide from an MM2FS simulation
SM-DS-SV **Single Material,** **Deformable Slide,** **Simulated Velocity**	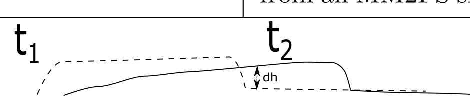 Change in shape and location of slide extracted from MM2FS simulation	

of the slide volume and the average slope, which is determined between the initial start and end depths of the slide. The velocity profile is chosen to be half-sinusoidal (in line with Harbitz (1992)), with the period $T = \frac{\pi}{2}\frac{R}{u_{max}}$, where R is the total run-out length, selected to be equal to the slide total length, $R = L + 2S$, where L is the 'length' of the slide, S the length over which the slide thickness tapers. The total run out distance consists of an acceleration phase, R_a and a deceleration phase, R_d, whereby $R_a = R_d = R/2$. The position of the slide, varies in time according to the relationship:

$$0 < t < T \begin{cases} x_s = x_0 + s(t)\cos(\varphi) \\ y_s = y_0 + s(t)\sin(\varphi) \end{cases} \tag{8}$$

where x_0, y_0 defines the start location and φ is the angle from the x-axis that the slide travels in, Acceleration phase:

$$s(t) = R_a\left[1 - \cos\left(\frac{u_{\mathrm{max}}}{R_a}t\right)\right], \quad 0 < t < T_a \tag{9}$$

Deceleration phase:

$$s(t) = R_a + R_d\left[\sin\left(\frac{u_{max}}{R_d}(t - T_a - T_c)\right)\right], \quad T_a < t < T. \tag{10}$$

The width and height of the resulting half-sinusoid can be adjusted by altering the estimated run out distance of the slide and the estimated maximum velocity, respectively. Slide dimensions are specific to each scenario and are discussed in section 3 and 4. The slide height remains constant as it travels over the bathymetry, whereas in the case of a deformable slide, the slide material will move under gravity according to local slope and changes in thickness.

2.4. Generation of meshes and three-dimensional domains

A three–dimensional mesh was generated using QGIS software (QGIS Development Team, 2009), *qmsh* (Avdis et al., 2018) and *Gmsh* (Geuzaine and Remacle, 2009). The spatial resolution at the coastlines of interest is 0.5 km, and 1 km at other coastlines, the resolution is linearly increased to 50 km furthest from the coastline. In the initial location of the submarine slide the spatial resolution is 2 km within a 80 km radius of the slide. Higher resolution is specified in shallow regions, and coarser resolution in regions of deep ocean, by varying the resolution according to the square–root of the bathymetry and gradient of the bathymetry. This is in order to capture the reduction in wavelength when tsunami enter shallower water. Combining these constraints on spatial mesh resolution results in mesh elements that have typical maximum edge lengths of 35 km. The mesh is composed of triangular elements across a two-dimensional surface and is extruded down radially to the depth of the bathymetry, with a single layer of elements, making this similar to a depth averaged approach (Mitchell et al., 2010; Wells et al., 2010; Hill et al., 2014). A consequence of this approximation is the requirement for a minimum water depth, here 10 m is chosen. Multiple layers have been used in Fluidity, to capture dispersion in Oishi et al. (2013) and in sensitivity tests in Smith et al. (2016) and Smith (2017). Future work can incorporate multiple layers into the three-dimensional Single Material approach presented here. Bathymetric data was obtained from the GEBCO 250 (IOC, 2008) dataset. The coastline is represented by the 0 m contour extracted from the GEBCO 250 dataset (IOC, 2008).

On the sea floor of the domain a no-normal flow boundary condition is applied except where a velocity boundary condition is instead being used to mimic the effect of the slide on the water during slide motion (Equation 6). A free surface boundary condition (see Smith et al. (2016)) is applied to the upper surface of the domain, but without movement of the mesh. The coastlines have a free-slip, no-normal flow boundary condition, which prevent inundation and reflect incoming waves. The minimum water depth in simulations is 10 m at the coastline, meaning that shoaling at depths less than 10 m, and inundation are not captured in the model. As the waves are not subject to the final shoaling that occurs, the wave amplitudes reported at the coastlines will be less than expected wave amplitudes on land. At the open boundaries surrounding the domain a 'stress-free' condition is used that allows the waves to freely flow out of the domain. The water has a density of 1000 $\mathrm{kgm^{-3}}$ and the kinematic viscosity tensor is isotropic and set to 1 $\mathrm{m^2s^{-1}}$. These 'eddy' viscosity values were selected in order to dampen any instabilities at the water surface, whilst being low enough to have a negligible effect on the overall waveform.

3. Model verification: test case in Gulf of Mexico

3.1. Set-up

The two-dimensional submarine slide scenario in the Gulf of Mexico, that is considered in Horrillo et al. (2013) and Smith et al. (2016), is here extended into three dimensions following Horrillo et al. (2013), who used the TSUNAMI3D model. TSUNAMI3D is a three-dimensional Navier–Stokes model for water and submarine slide that builds on the classical VoF formulation of Hirt and Nichols (1981) to track both the water surface and slide interface on a structured grid with a 3rd order finite difference scheme to solve the incompressible Navier–Stokes system. The VoF method determines regions containing water and slide material, with corresponding cell-weighted values of physical properties (density and viscosity) used in the momentum equation, in a very similar manner to the MM2FS approach employed in this work. TSUNAMI3D uses a simplified treatment of the free surface: the free surface in each column of cells is treated as horizontal, and consequently, wave breaking cannot be modelled. The water and slide are modelled as two incompressible, Newtonian fluids. For the full-scale tsunami simulations in a vertical two-dimensional slice domain TSUNAMI3D is configured to only employ two cells in the "third" dimension (Horrillo et al., 2013). This submarine slide is a hypothetical scenario based on geomorphological evidence for an historic slide of that volume in the same area, with parameters described in Table 2. The location and direction of failure (heading) of the slide are shown in Figure 1A and the three-dimensional mesh is shown in Figure 1B.

To simulate a three-dimensional simplified rigid slide in this test case, the length of the slide, L, and thickness, h, are kept consistent with the two-dimensional simulations in Smith et al. (2016) and Horrillo et al. (2013) and the maximum slide height is then adjusted to give the same cross sectional area. The shape is shown in Figure 1C. The two-dimensional slide thickness is maintained to a distance of $\pm$B/2 perpendicular to the transect line, in both directions, where B is the slide width, 18.1 km (Horrillo et al., 2013). A smoothing factor, $h_{\max}\exp - (0.3(\frac{y'}{B})^4)$, is applied as a function of perpendicular distance, y', to the transect line. This smoothing is in line with Harbitz (1992) and Hill et al. (2014), except the factor of 0.3 which has been altered from 2.0, to ensure a consistent slide volume with Horrillo et al. (2013) of 26.7 km^3 (See Table 2 and Figure 1C). The horizontal axis of the two-dimensional domain forms the transect through the centre of the slide, along the bearing of slide failure.

The SM-DS-SV approach is modelled in three dimensions using the Boussinesq set-up in Fluidity, as described in Section 2. For the SM–RS–EV approach, a slope angle is required in Equation (7) to calculate the estimated velocity profile. The local continental slope is averaged over the length of the slide and to a run–out distance of one slide length (Table 2). The acceleration of the slide in the SM-RS-EV approach is altered to match the acceleration of the slide in Horrillo et al. (2013) (Figure 2). The timestep for all three approaches modelled in this test case is set at 1 s.

Table 2: Parameters for three-dimensional SM-RS-EV simulation in Gulf of Mexico. Where L is slide length and S is the smoothing length described in Section 4.1.

Long, Lat of headwall	Heading	Slope Angle	Maximum velocity (m/s)	Volume (km^3)	Slide thickness (m)	L,S,Width (km)
95:40:35W, 27:42:59N	168.15°	0.69°	41	26.7	96.65	16,9.4,18

3.2. Results

For each simulation using Fluidity (the SM-RS-EV, SM-RS-SV and SM-DS-SV approaches) the generated waves are compared to TSUNAMI3D (Horrillo et al., 2013) at 7 and 10 minutes after slide motion has initiated (Figure 3). At 7 minutes there is a reduction in the maximum wave amplitude of about 50% in both TSUNAMI3D and Fluidity's SM-DS-SV approach in three dimensions compared to the maximum wave amplitudes the models predict in two dimensions (Horrillo et al., 2013; Smith et al., 2016), due to geometric/radial spreading, showing the importance of performing three-dimensional modelling.

In three dimensions, there is a good match between the three Fluidity approaches and TSUNAMI3D (Figure 3). TSUNAMI3D predicts a maximum peak–to–trough amplitude of 44 m. At this time, the SM-RS-EV and SM-RS-SV approaches produce almost identical wave forms to each other, predicting a peak–to–trough amplitude of 49 m. The SM-DS-SV approach predicts a smaller peak–to–trough amplitude of 37 m. Although the positive wave height produced by the SM–DS–SV approach is larger than for the SM–RS approach, the waves generated in the SM–RS approach have a deeper trough, resulting in a larger peak–to–trough amplitude. TSUNAMI3D's peak–to–trough amplitude falls within the range of Fluidity peak–to–trough amplitudes (35–49 m). At 7 minutes, the best match to TSUNAMI3D in terms of maximum and minimum wave amplitude is the SM-DS-SV approach. This is expected as the slide modelled in TSUNAMI3D also deforms, allowing the slide length to increase. The SM–DS–SV approach generates greater wave amplitudes than the SM–RS–EV and SM–RS–SV approaches because the deformation of the slide causes an increase in slide thickness at the front of the slide.

At 10 minutes there is still a qualitatively good match between TSUNAMI3D and all Fluidity approaches. Although Horrillo et al. (2013) do not give quantitative details of wave heights, the maximum wave amplitude in TSUNAMI3D appears to be under 20 m (and the minimum wave amplitude greater than -30 m). All Fluidity approaches produce a maximum wave height of 12.5–13 m. In TSUNAMI3D the maximum wave height occurred at 7 minutes and by 10 minutes, the wave height had decreased. In Fluidity maximum wave heights are observed during the slide acceleration phase at 8 min 28 s, 8 min 32 s, and 7 min 40 s for SM-RS-EV, SM-RS-SV and SM-DS-SV approaches respectively, which is in agreement with TSUNAMI3D. Over the course of the simulation, the SM-RS-EV approach predicts a maximum wave height that is 16 % lower than the maximum wave height that the SM-DS-SV approach predicts. Compared to TSUNAMI3D all approaches slightly underestimate the maximum positive wave amplitude, future work could investigate whether this could be due to the exclusion of the tangential applied stress (skin friction drag) in these SM approaches in three dimensions.

4. Atlantic Ocean Scenarios

Considering the potential for another tsunamigenic slide in the Norwegian-Greenland Sea, two hypothetical submarine slide events at the continental margin, west of Scotland and Ireland, on the edge of the Atlantic Ocean, were simulated in three dimensions. These locations were identified as having the potential to fail in the future, based on sedimentological evidence of historic slides and evidence of high sedimentation rates. Several other locations in the Norwegian-Greenland Sea have also been identified as having the potential to fail, but the two scenarios investigated here were chosen due to their proximity to land. The two slides occur on either side of the Rockall Trough basin (seen in Figure 4). The Peach Slide Complex is found on the eastern slope of the trough, on the Barra Fan, and the Rockall Bank slide scenario occurs on the opposite slope on the trough, on the western side.

Submarine slide geometry and motion for the hypothetical scenarios in the Norwegian–Greenland Sea were estimated using typical dimensions for submarine slides in the Atlantic Ocean (Hühnerbach and Masson, 2004). Scenario 1, named Rockall Bank, is based on the occurrence of a past failure on the eastern flank (Roberts, 1972; Georgiopoulou et al., 2013; Salmanidou et al., 2017). Scenario 2, named Peach Slide, is located on the Barra-Donegal Fan where the complex shows evidence of about four separate submarine slide events with slide volumes ranging from 135–673 km^3 (Holmes et al., 1998). The two slides have motions in approximately opposite directions. This will allow the effect of slide direction on the waves generated to be established. Volumes of historical submarine slides in this area are not well constrained. Salmanidou et al. (2015) considered slides on the Rockall bank with volumes ranging from 265-765 km^3. For both scenarios, failure volumes of 100 km^3 are used and are considered conservative estimates, not "worse case" scenarios.

4.1. Set-up

The dimensions of the hypothetical slides considered in this section must be estimated. The rationale for estimating slide dimensions is based on the previous work of Harbitz (1992), Løvholt et al. (2005) and Hill et al. (2014). In the model, the slide thickness h_s is defined as:

$$h_s = \begin{cases} h_{\max}\Big(\exp - (2(\frac{x'+S+L}{S})^4) - (2\frac{y'}{B})^4\Big) & \text{for} - (L+2S) < x' < -(L+S) \\ h_{\max}\Big(\exp - (2\frac{y'}{B})^4)\Big) & \text{for} - (L+S) \leqslant x' < -S \\ h_{\max}\Big(\exp - (2(\frac{x'+S}{S})^4) - (2\frac{y'}{B})^4)\Big) & \text{for} - S \leqslant x' < 0 \end{cases} \tag{11}$$

where the slide has dimensions of maximum height, $h_{\max}$, length, L, and width, B. A smoothing length, S, is used along the edges of the slide to avoid sharp edges, which give rise to numerical oscillations, as described in Harbitz (1992). x' and y' are the transverse and longitudinal coordinates, respectively, on a local plane aligned in the direction of slide motion φ:

$$x' = (x - x_s)\text{cos}\varphi + (y - y_s)\text{sin}\varphi \tag{12a}$$

and

$$y' = (x - x_s)\text{sin}\varphi + (y - y_s)\text{cos}\varphi \tag{13a}$$

where x_s and y_s are the coordinated of the back of the slide, and x and y are the model coordinates in the Universal Transverse Mercator projection (UTM zone 30N).

Using these slide dimensions, $h_{\max}$, L and B, gives a total volume of the slide, V:

$$V = 0.9Bh_{\max}(L + 0.9S), \qquad \text{(Harbitz, 1992).} \tag{14a}$$

Values for V, L, S, B and $h_{\max}$ are determined by fitting a power law to data for the Atlantic Ocean collated in Hühnerbach and Masson (2004) and choosing dimensions that fit the line based on four principles:

1. a desired slide volume, V
2. S, the smoothing/tapering length is defined as $L/2$

3. a relationship between V and B determined from Hühnerbach and Masson (2004):

$$V = 0.0335 \times B^{2.373} \quad (R^2 = 0.9) \tag{15}$$

4. a relationship between L and B determined from Hühnerbach and Masson (2004):

$$(L + 2S) = 1.377 \times B^{-1.11} \quad (R^2 = 0.9) \tag{16}$$

where R^2 is a measure of how well the line of best fit fits the observational data. The resulting three–dimensional slide is shown in Figure 4B.

The MM2FS approach (Smith et al., 2016) is used to model the Rockall Bank and Peach slides in two dimensions, modelling the slide and water as viscous fluids. Both two-dimensional slide geometries are determined from a three-dimensional volume of 100 km^3. Fitting a power law to the data for slides the Atlantic Ocean in Hühnerbach and Masson (2004) and choosing slide dimensions to fit the line, results in a slide length of 58 km, a maximum slide thickness of 91 m (this agrees with estimated headscarp heights from Georgiopoulou et al. (2013) of 50–150 m) and a slide width of 29.1 km (set out in Table 3). Two-dimensional multi-scale meshes are used (Figure 5). The slide shape through time is extracted from MM2FS simulations (Smith et al., 2016) for use in the SM-DS-SV approach (Figures 6 and 7). The displacement of the slide's centre of mass is extracted for the SM-RS-SV approach. For the Rockall Bank scenario, the SM-DS-SV approach (R1) and SM-RS-SV (R2) approach are applied, along with two different estimated velocity profiles for the SM-RS-EV approach (R3 and R4). One velocity profile has a maximum velocity of 74 ms^{-1} (for constant slope 2.2°, R4) and the other has a maximum velocity of 29 ms^{-1} (constant slope 0.7°, R3), and consequently a much lower initial acceleration (Figure 8). The maximum

Table 3: Parameters for three dimensional simulations, Atlantic Ocean scenarios. The average slope was used to calculate the maximum velocity of the slide.

Scenario Name	Rockall Bank				Peach
Simulation Name	R1	R2	R3	R4	P1
Fluidity Approach	SM-DS-SV	SM-RS-SV	SM-RS-EV	SM-RS-EV	SM-DS-SV
Volume (km^3)	100				
Slide thickness (m)	91				
L,S, Width (km)	29, 14.5, 29.1				
Run-out length (km)	58				
Headwall Lon, Lat	13:15:13.86W, 57:10:16.95N				9:08:26.50W, 56:45:10.79N
Heading (°)	170				340
Average Slope (m/m)	0.7			2.2	0.67
Max Velocity (m/s)	Simulated		29	74	Simulated

velocities for these velocity profiles were obtained through extracting bathymetry data, the range of slopes found on the Rockall Bank (0.7–2.2 depending on the location and length of the slope) and the force-balance question in section 2. Comparing waves generated by slides with different accelerations and maximum velocities allows the importance of slide deformation and velocity/acceleration to be considered. For context, the slide in the Gulf of Mexico example has a maximum velocity of approximately 45 ms^{-1} (Figure 2). For the Peach slide the SM-DS-SV approach (P1) is applied for comparison with the Rockall Bank using the same approach (SM-DS-SV) to investigate the effect of direction on coastal hazard (R1).

The meshes for the Rockall Bank and Peach Slide have 151892 and 150257 nodes, respectively (Figure 9). The timestep for the SM-RS-EV approach is 3 s (R3, R4), and for the SM-RS-SV approach (R2) and for the SM-DS-SV approach the timestep is 1 s (R1). For the SM-RS-EV approach (R3, R4) there is a negligible difference in the resultant waves using a timestep of 1 s and 3 s. However for the SM-DS-SV (R1, P1) and SM-RS-SV (R2) approaches, a smaller timestep of 1 s is required to ensure stability due to sharper changes in vertical velocity across shorter length scales compared to the smoothed rigid slide. Several numerical wave gauges are placed in the domain to measure the variation of fields (including free surface height and velocities) at specific geographic locations; e.g., between the slide and the coastlines of Ireland, Northern Ireland and Scotland (Figure 4), and located radially around the slide locations and the UK coast.

4.2. Results and Discussion

Simulations were run in parallel, on 48-256 cores, for a total simulation time of 240 hours. The SM-RS-EV approach (R3, R4) took approximately 4000–4500 CPU hours (no. cores $\times$ time to complete), the SM-RS-SV approach (R2) took about 1.5 times as long, at 6500 CPU hours and the SM-DS-SV (R1, P1) approach took approximately 4 times as long as the SM-RS-EV approach (R3, R4) at 18000 CPU hours. This is mostly due to the smaller timestep needed in the SM-DS-SV approach (R1, P1) and the more complex velocity patterns present in the SM-RS-SV (R2) and SM-DS-SV (R1, P1) approaches compared to the SM-RS-EV approach (R3, R4). The SM-DS-SV approach (R1, P1) also required additional input files and interpolations of the slide shape in space and time, adding additional overhead. Throughout the simulations maximum wave amplitudes reach between 16 and 26 m in the wave generation region. However, for the majority of the domain wave amplitudes are less than 10 m. Initially the results produced for the Rockall Bank scenario using the SM-DS-SV, SM-RS-SV, and SM-RS-EV approaches are considered (R1-R4). In this section the effect of slide velocity, acceleration and deformation on the generated wave are considered.

4.2.1. Rockall Bank: Comparison of model approaches, R1, R2, R3, R4

The wave pattern generated over time by the SM-RS-SV and SM-DS-SV approaches for the Rockall Bank is presented (Figure 10). Waves propagate from the generation zone and their amplitudes decay with increasing distance because of geometric spreading and dispersion. As the waves propagate they are diffracted around various seamounts, and later on, refracted around the Outer Hebrides. These wave processes create constructive and deconstructive wave interference. Waves hit the continental slope at ∼30 mins and undergo shoaling (Figure 10). Shoaling leads to a decrease in wavelength and wave speed, and an increase in wave amplitudes. Following shoaling, both waves decay in amplitude whilst travelling over the continental shelf and consequently waves between 1–10 m in amplitude reach just offshore of the coastline (Figure 11). Waves reach land around 1 hour after the initiation of slide motion and the first wave to reach land is a peak, and is followed by a trough. Waves greater than 1 m in amplitude reach the coast of the mainland north western Irish coast (Figure 11). The Outer Hebrides experiences wave heights of greater than 10–20 m (depending on the use of the SM-RS-SV approach or the SM-DS-SV approach, taking the brunt of the waves and sheltering much of mainland Scotland from experiencing wave heights greater than a few metres. The north coast of Scotland records waves 0.5–5 m in amplitude. Further afield, waves greater than 1 m in amplitude reach the coast of Iceland and the Faroe Islands for both scenarios (Figure 11).

4.2.2. Effect of slide deformation: SM-DS-SV (R1) vs. SM-RS-SV (R2)

The SM-RS-SV (R2) and SM-DS-SV (R1) approaches exhibit very similar wave patterns within the first 10 minutes after slide initiation (Figure 10). This suggests that the wave pattern is primarily controlled by the slide motion, since the SM-RS-SV (R2) approach assumes the slide is moving at the same speed as the slide's centre of mass in the SM-DS-SV (R1) approach. The differences between the results can be attributed to the internal slide deformation that occurs in the SM-DS-SV (R1) approach and not in the SM-RS-SV (R2) approach. After the first 10 minutes, a more complex wave pattern (more peaks and troughs) is produced by the SM-DS-SV approach. The SM-DS-SV (R1) approach accounts for internal slide deformation that generates additional short wavelength perturbations within the long wavelength signal. This leads to velocity variations over the length of the slide in the SM-DS-SV approach contributing to wave generation in additional locations. In the SM-RS-SV (R2) approach the slide surface is smooth, there is no internal deformation, and therefore vertical velocity is only induced at the front and back of the slide (elsewhere the thickness is constant). The SM-RS-SV (R2) approach generates waves with lower amplitudes than the SM-DS-SV (R1) approach (Figure 11), which suggests the deformation of the slide is contributing to increased wave heights. Another explanation for the difference in wave heights generated by the two different approaches is that the velocity of the slide in the SM-RS-SV (R2) approach (which uses the velocity of the centre of mass on the slide) is not a good approximation for the side motion in the SM-DS-SV (R1) approach, in which different sections of the slide will move at different velocities.

In this example, slide deformation leads to an increase in wave heights at the coastline. This increase in wave amplitude depends on the location of the wave gauge, but in general, the SM-DS-SV approach produces ∼30–50% higher waves than the SM-RS-SV approach and two times greater maximum wave amplitudes. These findings are in agreement with Grilli and Watts (2005) who report increases in wave amplitudes at wave gauges of between 13–35% and an increase in wave run up of a factor of 2–3 for deformable slides compared to rigid slides. Grilli and Watts (2005) conclude that intense slide deformation at shallow water depths significantly increases the coastal hazard the waves pose. However, other studies have found that slide deformation does not have a significant effect on the generated wave amplitude compared to rigid slides (Løvholt et al., 2015), because the slide accelerates too fast into deeper water for the deformation to influence the wave generation. In the scenarios considered here, slide deformation does contribute to wave generation. Some studies have found that slide deformation leads to decreased wave amplitudes (Watts, 1997; Ataie-Ashtiani and Najafi-Jilani, 2008; Kirby et al., 2016). However, the majority of these studies consider submarine slides at laboratory scale, higher slope angles (15–60°) and slides that are smaller, have a higher thickness to length ratio and different slide rheologies (e.g granular and confined granular) (Watts, 1997; Ataie-Ashtiani and Najafi-Jilani, 2008). Although the example in Kirby et al. (2016) is full scale and three dimensional, the scenario considered two separate, but simultaneous slides, whose combined effects generate the wave, and therefore it is difficult to compare the results with the single slide scenarios considered here.

4.2.3. Effect of slide velocity and acceleration: SM-RS-EV using different velocity profiles (R3 vs. R4)

The resultant waves from two rigid slides moving with two different velocities profiles are also considered (Fig. 11). The wave heights predicted by the SM-RS-EV simulation, representing a slow slide moving with a maximum velocity of 29 ms^{-1}

(R3) are, in places, a fraction of (or even negligible compared to) the wave amplitudes generated by the rigid fast slide moving with a maximum velocity of 74 ms^{-1} (R4, fast). The increase in maximum velocity is approximately a factor of 2.5, but the waves generated can be a factor of 3–7 times bigger. This suggests that the wave is very sensitive to the slide and acceleration of the slide generating the waves. At the coast, the maximum wave recorded at each location is 2–20 times larger for the faster slide (R4), depending on precise location. This strong dependence of wave amplitude on slide velocity and acceleration is in agreement with many previous findings, e.g. Wiegel (1955); Watts (1998, 2000); Watts et al. (2000); Ward (2001); Tinti et al. (2001); Haugen et al. (2005); Løvholt et al. (2005); Harbitz et al. (2006).

4.2.4. Application to coastal hazard assessments

Waves with amplitudes of up to 10 m from the Rockall Bank and Peach slides reach the coastline after undergoing shoaling on the continental slope. The highest waves that reach the coast are recorded along the west coast of Ireland for both slides, with peak heights of 10 m for the Peach slide and around 4 m for the Rockall slide. Just offshore the Northern Irish city of Londonderry/Derry waves are predicted between 2–4.5 m high for Peach Slide and 1.2–2 m high from Rockall Bank slide (Figure 12). The city is sheltered by the surrounding coastline and therefore is not affected by waves of high amplitude. However, in Lough Foyle, further shoaling at shallow water depths may result in increased wave amplitudes. Wave heights are generally low (<1 m) along the south-western Scottish mainland coast, but start to peak again around the islands of Arran, and Islay (point e on Fig. 4). The Outer Hebrides experience similar height waves from both the Peach and Rockall slides, but with slightly higher peaks for the Peach scenario (just over 4m vs. just over 3 m respectively). Along the northern coast of Scotland (f to g on Fig. 4) the Rockall scenario produces large maximum wave heights, but these are generally low (peak 2.25 m) with the Peach slide producing a maximum wave height of 2 m.

The Peach slide produces larger peak amplitude waves in the direction of slide travel at 100 km distance from the slide stating point, but these seem to rapidly diminish in size (Fig. 12). At 200 km from the slide start point both slide scenarios produce similar sized peak waves, that are again aligned with the slide direction. The Rockall slide appears to have a very clear focus of energy with clear dips in wave amplitude perpendicular to slide direction. In contrast, the energy from the Peach slide spreads more evenly in all directions (but with a peak aligned to the slide direction).

4.2.5. Limitations

There are limitations to the results presented here. Firstly, the MM2FS simulations show that some slide deformation occurs at scales on the order of 100 m. However, the three–dimensional simulations have a minimum mesh resolution in the slide region of 2 km, meaning that the slide is described by approximately 423 elements (for all approaches). Therefore the three-dimensional SM-DS-SV (R1, P1) simulations may be missing, or smoothing out, more detailed information about the slide geometry. Mesh resolution studies are recommended to investigate to what extent this affects the waves generated. Resolution studies have previously only been completed for the SM-RS-EV approach simulations by Hill et al. (2014), where it was concluded that multi-scale meshes with the same minimum and maximum edge lengths as those considered here were able to accurately represent observed run-up height estimates.

Secondly, the slides here are also assumed to be constant width and, in reality, there will be some spreading or funnelling of the slide laterally. The velocity boundary condition, that mimics the slide deformation and motion, is also applied uniformly along the width, whereas in reality there will be differences in bathymetry across the width of the slide which will lead to changes in deformation along the width of the slide. If deformation is permitted in three dimensions, this may also have an effect on the difference between waves amplitudes generated by rigid and deformable slides. In previous experimental work (Watts et al., 2005), the slide width has been found to have an important effect on wave amplitude, therefore a more thorough investigation including modelling of slides that are able to spread laterally, should be performed in order to establish to what degree this has an effect on the generated wave. If, in the results presented here, thickening of the front of the slide is increased compared to if the slide was allowed to spread laterally, this could account for some of the increased wave heights seen by the SM-DS-SV approach compared to the SM-RS-SV approach.

Lastly, the configuration employed here does not allow inclusion of shoaling and inundation in areas of bathymetry shallower than 10 m depth near to the coastlines. This means that wave heights recorded at the wave gauges are likely underestimated as the final shoaling and funnelling is not modelled. Inundation modelling within Fluidity is too computationally expensive to fall within the scope of this study. An alternative approach is to use another model, such as TELEMAC or Thetis (Kärnä et al., 2018; Pan et al., 2019, 2020), to simulate inundation by forcing it with the output of Fluidity. This is recommended as future work to fully establish the magnitude of the underestimation of wave amplitudes.

5. Conclusions

A three-dimensional Navier-Stokes model (using the Boussinesq approximation) has been presented that simulates the tsunami waves generated by submarine slides.

The framework has been used to investigate the role of slide deformation in wave generation. In the model, the water motion was driven by a boundary condition applied at the sea floor. The boundary condition mimicked the effect of the slide motion on the water column, and was determined in three different ways, using 1) a submarine slide modelled as a viscous fluid, without fixed shape, moving under gravity, 2) a rigid submarine slide, moving with a velocity profile extracted from (1) and 3) a rigid submarine slide, moving with a prescribed analytical velocity profile. For methods 1) and 2) a two-dimensional simulation was used to model both the submarine slide and water as viscous fluids. The simulations were then 'coupled'; i.e., outputs (change in shape and motion of submarine side material) from a 2D simulation of viscous fluids was extracted and used as a boundary condition for the three-dimensional simulation of water.

We verified our model, framework and coupling methodology by comparing our results to a previous simulation of a tsunamigenic submarine slide in the Gulf of Mexico. We then showed the difference in risk due to the consideration of slide deformation for hypothetical submarine slides around the UK (with the limitation of modelling wave propagation to 10 m depth off shore). Shoaling at depths less than 10 m, and inundation are not captured in the model. As the waves are not subject to the final shoaling that occurs, the wave amplitudes reported at the coastlines will be less than the expected wave amplitudes on land.

Comparisons were made between an approach that accounts for deformation of submarine slides (1) and an approach that used a rigid slide that moved according to prescribed motion (3). Slides moving with greater velocity and acceleration produce larger amplitude waves and results show there is a strong dependence of wave amplitude on velocity and acceleration. Approaches that do not consider slide deformation appear to provide good estimates compared to approaches that do account for slide deformation. However, it is still imperative to use accurate estimates for the slide velocity and position throughout the wave generation process, because the wave characteristics are very sensitive to these parameters. Since it is difficult to measure submarine slide velocities as they occur, numerical modelling of slides is a useful tool to obtain good estimates for these parameters, which could then be used as an input for a ocean-scale model.

In this work, slide deformation was modelled assuming that the slide behaved as a viscous fluid. The deformation of slide material caused slide thickness to increase and decrease along the length of the slide. The slide thickness increased up to 4 times larger than its starting thickness, and there is a corresponding decrease in thickness at other areas of the slide in accordance with volume conservation. The slope varies along the length of the slide which causes material to move at different velocities, resulting in local thickening and thinning. Results presented here found that changes in slide thickness contribute to a 30-50% increase in wave height for a slide that deforms compared to a rigid slide. However, modelling the slide as a viscous fluid may not result in the most accurate representation of slide dynamics and future work should investigate more. Furthermore, lateral spreading of the slide is not considered in this study and this could alter the effect of slide deformation, as the slide material spreads sideways. Multi-material simulations presented here indicate that components of slide deformation that occur at shallower depths, on the steepest slopes and involving the largest volume are more energetic than deformation at other sections of the slide and contributes most to wave generation. This work offers a new methodology for simulating oceanic-scale tsunamis caused by submarine slides within the same numerical framework, without recourse to coupling several different models together. In this study two–dimensional simulations were required to test the model, but in future simulations, the slide dynamics can be estimated given information about the slope angle and slide geometry. It provides the possibility for exploring the risk posed by tsunamigenic submarine slides, which threaten coastlines not normally thought to be prone to tsunamis.

Future work should model slides that spread laterally, and investigate the effect this has on wave amplitudes and on the relative significance of slide deformation. The effect of lateral spreading on the conclusions drawn here is unknown but potentially significant.

6. Acknowledgements

JH, GC and MDP acknowledge funding from NERC under project (NE/K000047/1). The authors would like to acknowledge the use of the Imperial College London HPC service. We would like to thank two anonymous reviewers for very helpful reviews that improved this manuscript.

7. References

References

Abadie, S., Morichon, D., Grilli, S., Glockner, S., 2010. Numerical Simulation of Waves Generated by Landslides using a Multiple-Fluid Navier–Stokes Model. Coastal Engineering 57, 779–794. URL: http://linkinghub.elsevier.com/retrieve/pii/S0378383910000396, doi:10.1016/j.coastaleng.2010.03.003.

Abadie, S.M., Harris, J.C., Grilli, S.T., Fabre, R., 2012. Numerical Modeling of Tsunami Waves Generated by the Flank Collapse of the Cumbre Vieja Volcano (La Palma, Canary Islands): Tsunami Source and Near Field Effects. Journal of Geophysical Research 117, C05030. URL: http://www.agu.org/pubs/crossref/2012/2011JC007646.shtml, doi:10.1029/2011JC007646.

AMCG, 2014. Fluidity manual v4.1.11, Imperial College London.

Assier-Radkiewicz, S., Einrich, P.H., Abatier, P.C.S., Avoye, B.S., 2000. Numerical Modelling of a Landslide-Generated Tsunami : The 1979 Nice Event. Pure and Applied Geophysics 157, 1707–1727.

Assier-Rzadkiewicz, S., Mariotti, C., Heinrich, P., 1997. Numerical Simulation of Submarine Landslides and their Hydraulic Effects. Journal of Waterway, Port, Coastal, and Ocean Engineering 123, 149–157. URL: http://ascelibrary.org/doi/abs/10.1061/(ASCE)0733-950X(1997)123:4(149).

Ataie-Ashtiani, B., Najafi-Jilani, A., 2008. Laboratory Investigations on Impulsive Waves caused by Underwater Landslide. Coastal Engineering 55, 989–1004. URL: http://linkinghub.elsevier.com/retrieve/pii/S0378383908000586, doi:10.1016/j.coastaleng.2008.03.003.

Ataie-Ashtiani, B., Shobeyri, G., 2008. Numerical Simulation of Landslide Impulsive Waves by Incompressible Smoothed Particle Hydrodynamics. International Journal for Numerical Methods in Fluids , 209–232URL: http://onlinelibrary.wiley.com/doi/10.1002/fld.1526/abstract, doi:10.1002/fld.

Avdis, A., Candy, A., Hill, J., Kramer, S., Piggott, M., 2018. Efficient unstructured mesh generation for marine renewable energy applications. RENEWABLE ENERGY 116, 842–856. URL: http://dx.doi.org/10.1016/j.renene.2017.09.058, doi:10.1016/j.renene.2017.09.058.

Bondevik, S., Løvholt, F., Harbitz, C., Mangerud, J., Dawson, A., Inge Svendsen, J., 2005a. The Storegga Slide Tsunami–Comparing Field Observations with Numerical Simulations. Marine and Petroleum Geology 22, 195–208. URL: http://linkinghub.elsevier.com/retrieve/pii/S0264817204001904, doi:10.1016/j.marpetgeo.2004.10.003.

Bondevik, S., Mangerud, J., Dawson, S., Dawson, A., Lohne, Ø., 2005b. Evidence for Three North Sea Tsunamis at the Shetland Islands Between 8000 and 1500 Years Ago. Quaternary Science Reviews 24, 1757–1775. URL: http://www.sciencedirect.com/science/article/pii/S0277379105000739, doi:10.1016/j.quascirev.2004.10.018.

Bornhold, B., Thomson, R., 2012. Tsunami Hazard Assessment Related to Slope Failures in Coastal Waters. Landslides–Types, Mechanisms and Modeling, edited by: Clague, JJ and Stead, D., Cambridge University Press , 108–120.

Bryn, P., Solheim, A., Berg, K., Lien, R., Forsberg, C., Haflidason, H., Ottesen, D., Rise, L., 2003. The Storegga Slide Complex; Repeated Large Scale Sliding in Response to Climatic Cyclicity, in: Locat, J., Mienert, J., Boisvert, L. (Eds.), Submarine Mass Movements and Their Consequences. Springer Netherlands. volume 19 of *Advances in Natural and Technological Hazards Research*, pp. 215–222.

Bugge, T., Belderson, R., Kenyon, N., 1988. The Storegga Slide. Philosophical Transactions of the Royal Society London 325, 357–388. URL: http://www.jstor.org/stable/10.2307/38068.

Capone, T., Panizzo, A., Monaghan, J.J., 2010. SPH Modelling of Water Waves Generated by Submarine Landslides. Journal of Hydraulic Research 48, 80–84. URL: http://www.tandfonline.com/doi/abs/10.1080/00221686.2010.9641248, doi:10.1080/00221686.2010.9641248.

Dawson, A., Long, D., Smith, D., 1988. The Storegga Slides: Evidence from eastern Scotland for a Possible Tsunami. Marine Geology 82, 271–276. URL: http://www.sciencedirect.com/science/article/pii/0025322788901466, doi:10.1016/0025-3227(88)90146-6.

De Blasio, F., Elverhøi, A., Issler, D., Harbitz, C., Bryn, P., Lien, R., 2005. On the Dynamics of Subaqueous Clay Rich Gravity Mass Flows—The Giant Storegga Slide, Norway. Marine and Petroleum Geology 22, 179–186. URL: http://linkinghub.elsevier.com/retrieve/pii/S0264817204001886, doi:10.1016/j.marpetgeo.2004.10.014.

Fine, I., Rabinovich, A., Bornhold, B., Thomson, R., Kulikov, E., 2005. The Grand Banks Landslide-Generated Tsunami of November 18, 1929: Preliminary Analysis and Numerical Modeling. Marine Geology 215, 45–57. URL: http://linkinghub.elsevier.com/retrieve/pii/S002532270400324X, doi:10.1016/j.margeo.2004.11.007.

Fine, I., Rabinovich, A., Kulikov, E., Thomson, R., Bornhold, B., 1998. Numerical Modelling of Landslide-generated Tsunamis with Application to the Skagway Harbor Tsunami of November 3, 1994, in: Proc. Int. Conf. on Tsunamis, Paris, pp. 211–223.

Gauer, P., Elverhøi, A., Blasio, F.D., 2006. On Numerical Simulations of Subaqueous Slides: Back-calculations of Laboratory Experiments. Norwegian Journal of Geology 86, 295–300.

Gauer, P., Kvalstad, T.J., Forsberg, C.F., Bryn, P., Berg, K., 2005. The Last Phase of the Storegga Slide: Simulation of Retrogressive Slide Dynamics and Comparison with Slide-Scar Morphology. Marine and Petroleum Geology 22, 171–178. URL: http://linkinghub.elsevier.com/retrieve/pii/S0264817204001874, doi:10.1016/j.marpetgeo.2004.10.004.

Georgiopoulou, A., Shannon, P.M., Sacchetti, F., Haughton, P.D.W., Benetti, S., 2013. Basement-controlled multiple slope collapses, Rockall Bank Slide Complex, NE Atlantic. Marine Geology 336, 198–214. URL: http://www.sciencedirect.com/science/article/pii/S002532271200312X, doi:10.1016/j.margeo.2012.12.003.

Geuzaine, C., Remacle, J.F., 2009. Gmsh: A 3-D finite element mesh generator with built-in pre- and post-processing facilities. International journal for numerical methods in engineering 79, 1309–1331. doi:10.1002/nme.2579.

Glimsdal, S., Pedersen, G.K., Harbitz, C.B., Løvholt, F., 2013. Dispersion of Tsunamis: Does it Really Matter? Nat. Hazards Earth Syst. Sci. 13, 1507–1526. URL: http://www.nat-hazards-earth-syst-sci.net/13/1507/2013/, doi:10.5194/nhess-13-1507-2013.

Grilli, S., Watts, P., 2005. Tsunami Generation by Submarine Mass Failure. I: Modeling, Experimental Validation, and Sensitivity Analyses. Journal of Waterway, Port, Coastal, and Ocean Engineering 131, 283–297.

Harbitz, C.B., 1992. Model Simulations of Tsunamis Generated by the Storegga Slides. Marine Geology 105, 1–21. URL: http://www.sciencedirect.com/science/article/pii/002532279290178K.

Harbitz, C.B., Løvholt, F., Pedersen, G., Masson, D.G., 2006. Mechanisms of Tsunami Generation by Submarine Landslides: A Short Review. Norsk Geologisk Tidsskrift 86, 255.

Harbitz, C.B., Løvholt, F., Bungum, H., 2014. Submarine landslide tsunamis: how extreme and how likely? Natural Hazards 72, 1341–1374. URL: http://link.springer.com/10.1007/s11069-013-0681-3, doi:10.1007/s11069-013-0681-3.

Haugen, K.B., Løvholt, F., Harbitz, C.B., 2005. Fundamental Mechanisms for Tsunami Generation by Submarine Mass Flows in Idealised Geometries. Marine and Petroleum Geology 22, 209–217. URL: http://linkinghub.elsevier.com/retrieve/pii/S0264817204001916, doi:10.1016/j.marpetgeo.2004.10.016.

Hiester, H.R., Piggott, M.D., Allison, P.A., 2011. The Impact of Mesh Adaptivity on the Gravity Current Front Speed in a Two-Dimensional Lock-Exchange. Ocean Modelling 38, 1–21. URL: http://www.sciencedirect.com/science/article/pii/S1463500311000060, doi:10.1016/j.ocemod.2011.01.003.

Hill, J., Collins, G.S., Avdis, A., Kramer, S.C., Piggott, M.D., 2014. How Does Multiscale Modelling and Inclusion of Realistic Palaeobathymetry Affect Numerical Simulation of the Storegga Slide Tsunami? Ocean Modelling 83, 11–25. URL: http://www.sciencedirect.com/science/article/pii/S1463500314001164, doi:10.1016/j.ocemod.2014.08.007.

Hill, J., Piggott, M.D., Ham, D.A., Popova, E.E., Srokosz, M.A., 2012. On the Performance of a Generic Length Scale Turbulence Model Within an Adaptive Finite Element Ocean Model. Ocean Modelling 56, 1–15. URL: http://www.sciencedirect.com/science/article/pii/S1463500312001023, doi:10.1016/j.ocemod.2012.07.003.

Hirt, C.W., Nichols, B.D., 1981. Volume of Fluid (VOF) Method for the Dynamics of Free Boundaries. Journal of Computational Physics 39, 201–225. URL: http://www.sciencedirect.com/science/article/pii/0021999181901455, doi:10.1016/0021-9991(81)90145-5.

Holmes, R., Long, D., Dodd, L.R., 1998. Large-Scale Debrites and Submarine Landslides on the Barra Fan, west of Britain. Geological Society, London, Special Publications 129, 67–79. URL: http://sp.lyellcollection.org/content/129/1/67, doi:10.1144/GSL.SP.1998.129.01.05.

Horrillo, J., Wood, A., Kim, G.B., Parambath, A., 2013. A Simplified 3-D Navier-Stokes Numerical Model for Landslide-Tsunami: Application to the Gulf of Mexico. Journal of Geophysical Research: Oceans 118, 6934–6950. URL: http://onlinelibrary.wiley.com/doi/10.1002/2012JC008689/abstract, doi:10.1002/2012JC008689.

Hühnerbach, V., Masson, D.G., 2004. Landslides in the North Atlantic and its Adjacent Seas: An Analysis of Their Morphology, Setting and Behaviour. Marine Geology 213, 343–362. URL: http://www.sciencedirect.com/science/article/pii/S0025322704002774, doi:10.1016/j.margeo.2004.10.013.

IOC, I., 2008. BODC, 2008. Centenary Edition of the GEBCO Digital Atlas, published on CD-ROM on behalf of the Intergovernmental Oceanographic Commission and the International Hydrographic Organization as part of the General Bathymetric Chart of the Oceans. British oceanographic Data Centre, Liverpool .

Jiang, L., LeBlond, P., 1992. The Coupling of A Submarine Slide and The Surface Waves Which It Generates. Journal of Geophysical Research 97, 12,731–12,744.

Jiang, L., LeBlond, P., 1993. Numerical Modeling of an Underwater Bingham Plastic Mudslide and the Waves Which it Generates. Journal of Geophysical Research 98, 303–317. URL: http://www.agu.org/pubs/crossref/1993/93JC00393.shtml.

Kärnä, T., Kramer, S.C., Mitchell, L., Ham, D.A., Piggott, M.D., Baptista, A.M., 2018. Thetis coastal ocean model: discontinuous Galerkin discretization for the three-dimensional hydrostatic equations. Geoscientific Model Development 11, 4359–4382. doi:10.5194/gmd-11-4359-2018.

Kirby, J.T., Shi, F., Nicolsky, D., Misra, S., 2016. The 27 April 1975 Kitimat, British Columbia, Submarine Landslide Tsunami: A Comparison of Modeling Approaches. Landslides , 1–14URL: http://link.springer.com/article/10.1007/s10346-016-0682-x, doi:10.1007/s10346-016-0682-x.

Laberg, J., Vorren, T., Mienert, J., Bryn, P., Lien, R., 2002a. The Trænadjupet Slide: A Large Slope Failure Affecting the Continental Margin of Norway 4,000 Years Ago. Geo-Marine Letters 22, 19–24. URL: http://www.springerlink.com/content/dhy3y2nepbwaa08b/abstract/, doi:10.1007/s00367-002-0092-z.

Laberg, J., Vorren, T., Mienert, J., Evans, D., Lindberg, B., Ottesen, D., Kenyon, N., Henriksen, S., 2002b. Late Quaternary Palaeoenvironment and Chronology in the Trænadjupet Slide Area Offshore Norway. Marine Geology 188, 35–60. URL: http://www.sciencedirect.com/science/article/pii/S0025322702002748, doi:10.1016/S0025-3227(02)00274-8.

Lee, C.H., Huang, Z., 2018. A two-phase flow model for submarine granular flows: With an application to collapse of deeply-submerged granular columns. Advances in water resources 115, 286–300.

Løvholt, F., Harbitz, C.B., Haugen, K.B., 2005. A Parametric Study of Tsunami Generated by Submarine Slides in the Ormen Lange/Storegga Area Off Western Norway. Marine and Petroleum Geology 22, 219–231. URL: http://linkinghub.elsevier.com/retrieve/pii/S0264817204001928, doi:10.1016/j.marpetgeo.2004.10.017.

Løvholt, F., Pedersen, G., Harbitz, C.B., Glimsdal, S., Kim, J., 2015. On the Characteristics of Landslide Tsunamis. Phil. Trans. R. Soc. A 373, 20140376. URL: http://rsta.royalsocietypublishing.org/content/373/2053/20140376, doi:10.1098/rsta.2014.0376.

Ma, G., Kirby, J.T., Shi, F., 2013. Numerical Simulation of Tsunami Waves Generated by Deformable Submarine Landslides. Ocean Modelling 69, 146–165. URL: http://www.sciencedirect.com/science/article/pii/S1463500313001170, doi:10.1016/j.ocemod.2013.07.001.

Ma, G., Shi, F., Kirby, J.T., 2012. Shock-Capturing Non-Hydrostatic Model for Fully Dispersive Surface Wave Processes. Ocean Modelling 43–44, 22–35. URL: http://www.sciencedirect.com/science/article/pii/S1463500311001892, doi:10.1016/j.ocemod.2011.12.002.

Masson, D.G., Harbitz, C.B., Wynn, R.B., Pedersen, G., Løvholt, F., 2006. Submarine Landslides: Processes, Triggers and Hazard Prediction. Philosophical Transactions of the Royal Society A: Mathematical, Physical and Engineering Sciences 364, 2009–2039. URL: http://rsta.royalsocietypublishing.org/cgi/doi/10.1098/rsta.2006.1810, doi:10.1098/rsta.2006.1810.

Mitchell, A.J., Allison, P.A., Piggott, M.D., Gorman, G.J., Pain, C.C., Hampson, G.J., 2010. Numerical Modelling of Tsunami Propagation with Implications for Sedimentation in Ancient Epicontinental Seas: The Lower Jurassic Laurasian Seaway. Sedimentology 228, 81–97. URL: http://www.sciencedirect.com/science/article/pii/S0037073810000692.

Oishi, Y., Piggott, M.D., Maeda, T., Kramer, S.C., Collins, G.S., Tsushima, H., Furumura, T., 2013. Three-Dimensional Tsunami Propagation Simulations Using an Unstructured Mesh Finite Element Model. Journal of Geophysical Research: Solid Earth 118, 2998–3018. URL: http://dx.doi.org/10.1002/jgrb.50225, doi:10.1002/jgrb.50225.

Pan, W., Kramer, S.C., Kärnä, T., Piggott, M.D., 2020. Comparing non-hydrostatic extensions to a discontinuous finite element coastal ocean model. Ocean Modelling , 101634doi:https://doi.org/10.1016/j.ocemod.2020.101634.

Pan, W., Kramer, S.C., Piggott, M.D., 2019. Multi-layer non-hydrostatic free surface modelling using the discontinuous galerkin method. Ocean Modelling 134, 68–83.

Parkinson, S.D., Hill, J., Piggott, M.D., Allison, P.A., 2014. Direct Numerical Simulations of Particle-Laden Density Currents with Adaptive, Discontinuous Finite Elements. Geosci. Model Dev. 7, 1945–1960. URL: http://www.geosci-model-dev.net/7/1945/2014/, doi:10.5194/gmd-7-1945-2014.

Piggott, M.D., Gorman, G.J., Pain, C.C., Allison, P.A., Candy, A.S., Martin, B.T., Wells, M.R., 2008. A New Computational Framework for Multi-Scale Ocean Modelling based on Adapting Unstructured Meshes. International Journal for Numerical Methods in Fluids 56, 1003–1015. URL: http://onlinelibrary.wiley.com/doi/10.1002/fld.1663/abstract, doi:10.1002/fld.1663.

QGIS Development Team, 2009. QGIS Geographic Information System. Open Source Geospatial Foundation. URL: http://qgis.osgeo.org.

Roberts, D., 1972. Slumping on the eastern margin of the Rockall Bank, North Atlantic Ocean. Marine geology 13, 225–237.

Salmanidou, D.M., Georgiopoulou, A., Guillas, S., Dias, F., others, 2015. Numerical Modelling of Mass Failure Processes and Tsunamigenesis on the Rockall Trough, NE Atlantic Ocean, in: The Twenty-fifth International Offshore and Polar Engineering Conference, International Society of Offshore and Polar Engineers. URL: https://www.onepetro.org/conference-paper/ISOPE-I-15-479.

Salmanidou, D.M., Guillas, S., Georgiopoulou, A., Dias, F., 2017. Statistical emulation of landslide-induced tsunamis at the rockall bank, ne atlantic. Proceedings of the Royal Society of London A: Mathematical, Physical and Engineering Sciences 473. URL: http://rspa.royalsocietypublishing.org/content/473/2200/20170026, doi:10.1098/rspa.2017.0026, arXiv:http://rspa.royalsocietypublishing.org/content/473/2200/20170026.full.pdf.

Shaw, B., Ambraseys, N.N., England, P.C., Floyd, M.A., Gorman, G.J., Higham, T.F.G., Jackson, J.A., Nocquet, J.M., Pain, C.C., Piggott, M.D., 2008. Eastern Mediterranean Tectonics and Tsunami Hazard Inferred from the AD 365 Earthquake. Nature Geosci 1, 268–276. URL: http://dx.doi.org/10.1038/ngeo151, doi:10.1038/ngeo151.

Smith, D., Shi, S., Cullingford, R., Dawson, A., Dawson, S., Firth, C., Foster, I., Fretwell, P., Haggart, B., Holloway, L., Long, D., 2004. The Holocene Storegga Slide Tsunami in the United Kingdom. Quaternary Science Reviews 23, 2291–2321. URL: http://www.sciencedirect.com/science/article/pii/S0277379104001003, doi:10.1016/j.quascirev.2004.04.001.

Smith, R.C., 2017. Numerical modelling of tsunami generated by deformable submarine slides. Ph.D. thesis.

Smith, R.C., Hill, J., Collins, G.S., Piggott, M.D., Kramer, S.C., Parkinson, S.D., Wilson, C., 2016. Comparing Approaches for Numerical Modelling of Tsunami Generation by Deformable Submarine Slides. Ocean Modelling 100, 125–140. URL: http://www.sciencedirect.com/science/article/pii/S1463500316000354, doi:10.1016/j.ocemod.2016.02.007.

Snelling, B.E., Collins, G.S., Piggott, M.D., Neethling, S.J., 2020. Improvements to a smooth particle hydrodynamics simulator for investigating submarine landslide generated waves. International Journal for Numerical Methods in Fluids .

Solheim, A., Berg, K., Forsberg, C., Bryn, P., 2005. The Storegga Slide Complex: Repetitive Large Scale Sliding with Similar Cause and Development. Marine and Petroleum Geology 22, 97–107. URL: http://linkinghub.elsevier.com/retrieve/pii/S0264817204001813, doi:10.1016/j.marpetgeo.2004.10.013.

Talling, P., 2013. Waves on the Horizon. Nature Geoscience 3, 179–179. URL: http://www.nature.com/nclimate/journal/v3/n3/pdf/nclimate1815.pdf.

Thomson, R.E., Rabinovich, A.B., Kulikov, E.A., Fine, I., Bornhold, B., 2001. On Numerical Simulation of the Landslide-Generated Tsunami of November 3, 1994 in Skagway Harbor, Alaska, in: Hebenstreit, G. (Ed.), Tsunami Research at the End of a Critical Decade. Springer Netherlands. volume 18 of *Advances in Natural and Technological Hazards Research*, pp. 243–282.

Tinti, S., Bortolucci, E., Chiavettieri, C., 2001. Tsunami Excitation by Submarine Slides in Shallow-water Approximation. Pure and Applied Geophysics 158, 759–797. URL: http://www.springerlink.com/index/10.1007/PL00001203, doi:10.1007/PL00001203.

Wagner, B., Bennike, O., Klug, M., Cremer, H., 2007. First Indication of Storegga Tsunami Deposits from East Greenland. Journal of Quaternary Science 22, 321–325. URL: http://onlinelibrary.wiley.com/doi/10.1002/jqs.1064/abstract, doi:10.1002/jqs.1064.

Ward, S.N., 2001. Landslide Tsunami. Journal of Geophysical Research 106, 11–201.

Watts, P., 1997. Water Waves Generated by Underwater Landslides. Ph.D. thesis. California Institute of Technology.

Watts, P., 1998. Wavemaker Curves for Tsunamis Generated by Underwater Landslides. Journal of waterway, port, coastal, and ocean engineering 124, 127–137.

Watts, P., 2000. Tsunami Features of Solid Block Underwater Landslides. Journal of Waterway, Port, Coastal, and Ocean Engineering 126, 144–152. doi:10.1061/(ASCE)0733-950X(2000)126:3(144).

Watts, P., Grilli, S., Tappin, D., Fryer, G., 2005. Tsunami Generation by Submarine Mass Failure. II: Predictive Equations and Case Studies. Journal of Waterway, Port, Coastal, and Ocean Engineering , 298–310URL: http://ascelibrary.org/doi/abs/10.1061/(ASCE)0733-950X(2005)131:6(298).

Watts, P., Grilli, S.T., Kirby, J.T., Fryer, G.J., Tappin, D.R., 2003. Landslide Tsunami Case Studies Using a Boussinesq Model and a Fully Nonlinear Tsunami Generation Model. Natural Hazards and Earth System Science 3, 391–402. URL: http://www.nat-hazards-earth-syst-sci.net/3/391/2003/, doi:10.5194/nhess-3-391-2003.

Watts, P., Imamura, F., Grilli, S., 2000. Comparing Model Simulations of Three Benchmark Tsunami Generation Cases. Science of Tsunami Hazards , 1–17.

Wells, M.R., Allison, P.A., Hampson, G.J., Piggott, M.D., Pain, C.C., 2005. Modelling Ancient Tides: the Upper Carboniferous Epi-Continental Seaway of Northwest Europe. Sedimentology 52, 715–735. URL: http://onlinelibrary.wiley.com/doi/10.1111/j.1365-3091.2005.00718.x/abstract, doi:10.1111/j.1365-3091.2005.00718.x.

Wells, M.R., Allison, P.A., Piggott, M.D., Hampson, G.J., Pain, C.C., Gorman, G.J., 2010. Tidal Modeling of an Ancient Tide-Dominated Seaway, Part 1: Model Validation and Application to Global Early Cretaceous (Aptian) Tides. Journal of Sedimentary Research 80, 393–410. URL: http://jsedres.geoscienceworld.org/content/80/5/393, doi:10.2110/jsr.2010.044.

Wiegel, R.L., 1955. Laboratory Studies of Gravity Waves Generated by the Movement of a Submarine Body. Transactions of the American Geophysical Union 36, 759–774.

Yavari-Ramshe, S., Ataie-Ashtiani, B., 2015. A Rigorous Finite Volume Model to Simulate Subaerial and Submarine Landslide-Generated Waves. Landslides , 1–19URL: http://link.springer.com/article/10.1007/s10346-015-0662-6, doi:10.1007/s10346-015-0662-6.

Yu, M.L., Lee, C.H., 2019. Multi-phase-flow modeling of underwater landslides on an inclined plane and consequently generated waves. Advances in Water Resources 133, 103421.

8. Supplementary Data

Example set-up files for the different approaches within Fluidity for each scenario can be found on the following link: https://dx.doi.org/10.6084/m9.figshare.3507734

Approach	Scenario	Dimenions	Filename
MM2FS	Gulf of Mexico	2D	**gom_2mat.flml**
SM-DS-SV	Gulf of Mexico	2D	**gom_SMDSSV_2D.flml**
SM-RS-SV	Gulf of Mexico	2D	**gom_SMRSSV_2D.flml**
SM-RS-EV	Gulf of Mexico	2D	**gom_SMRSEV_2D.flml**
SM-DS-SV	R1 - Rockall Bank	3D	**rockall_SMDSSV.flml**
SM-RS-SV	R2- Rockall Bank	3D	**rockall_SMRSSV.flml**
SM-RS-EV	R3- Rockall Bank	3D	**rockall_SMRSEV.flml**

extract slide shape.py can be used to extract the slide thickness from the output of an MM2FS simulation.

9. Figures

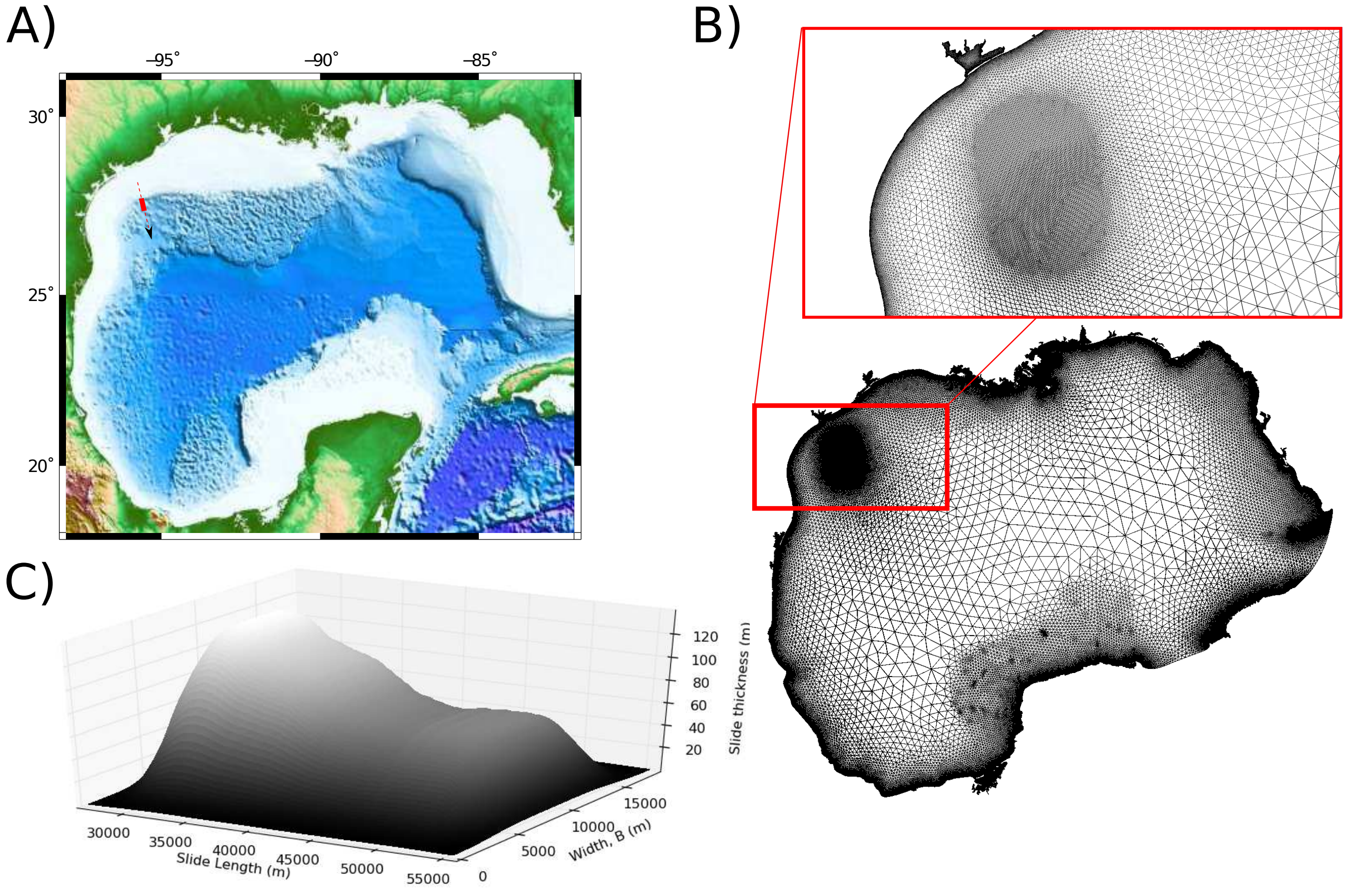

Figure 1: Model setup for the Gulf of Mexico verification test. A) Map of the Gulf of Mexico, including location of slide (rectangle) and direction of slide motion (dashed arrow). B) Overview of the mesh (bottom) with enlargement of the mesh in the region of the slide showing the increased resolution. C) Three-dimensional shape of the slide used in the simulations.

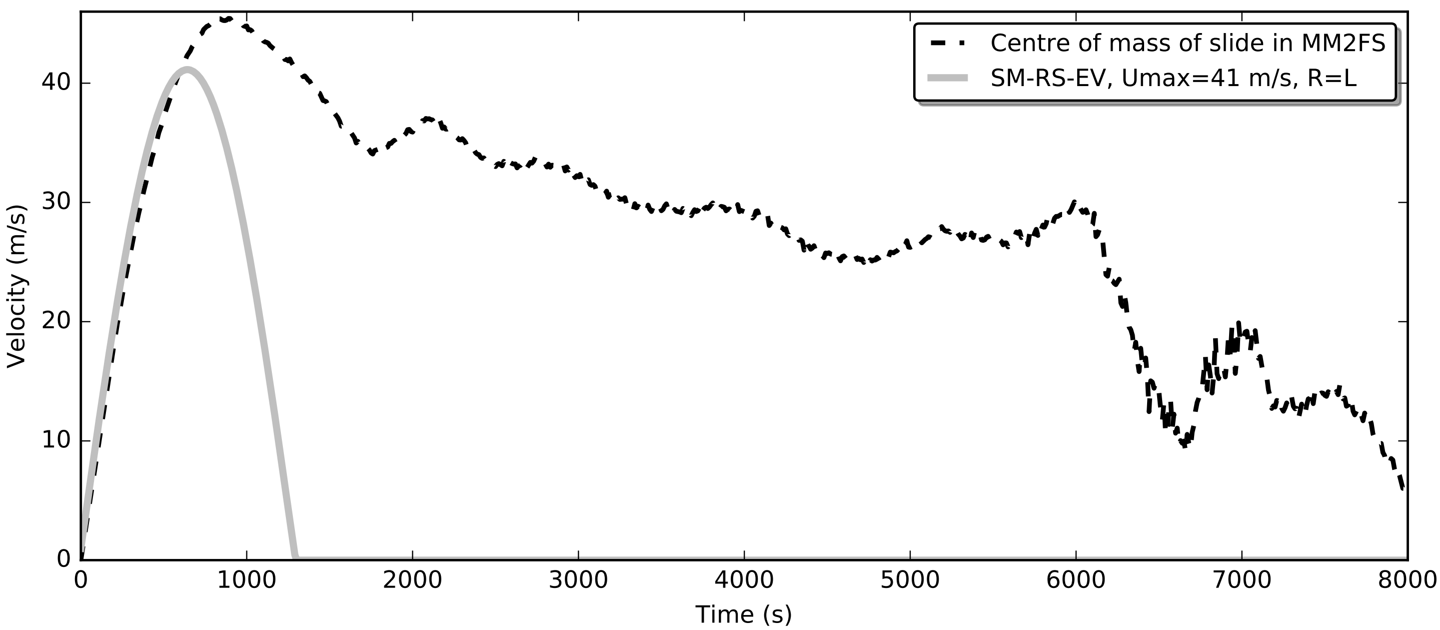

Figure 2: Comparison of velocity profiles for the SM-RS-EV approach (for the velocity of the slide's centre of mass in the MM2FS approach, dashed line), and for the SM-RS-SV approach with maximum velocity 41m/s (grey line). Although the velocity profiles are not similar after the first 1000s, the acceleration of the slides in the early part of slide movement are well matched, and it is this initial acceleration that is important for wave generation.

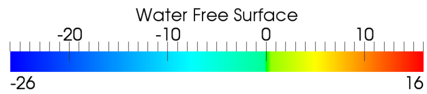

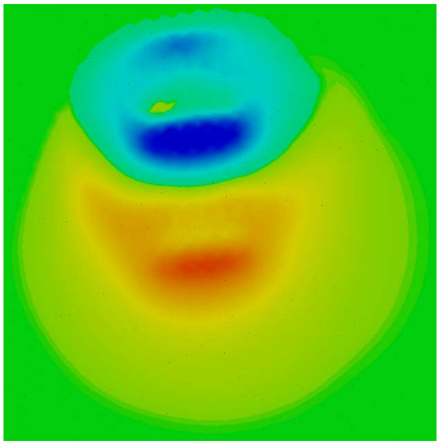

(a) SM-RS-EV, 7 mins

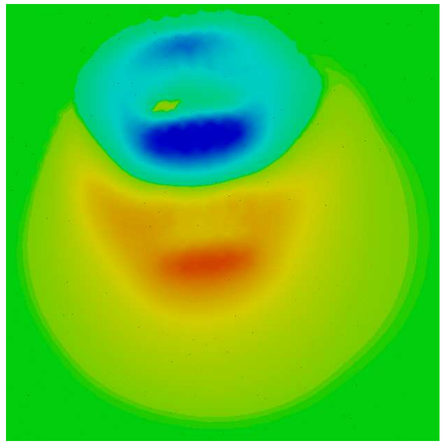

(b) SM-RS-SV, 7 mins

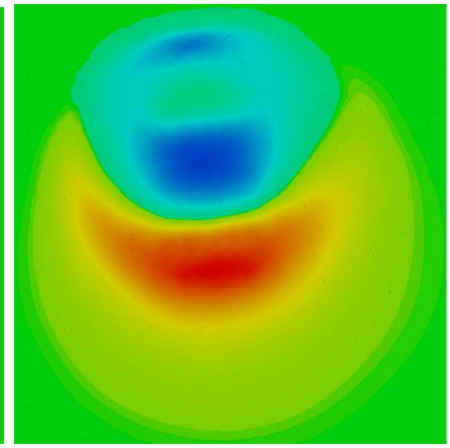

(c) SM-DS-SV, 7 mins

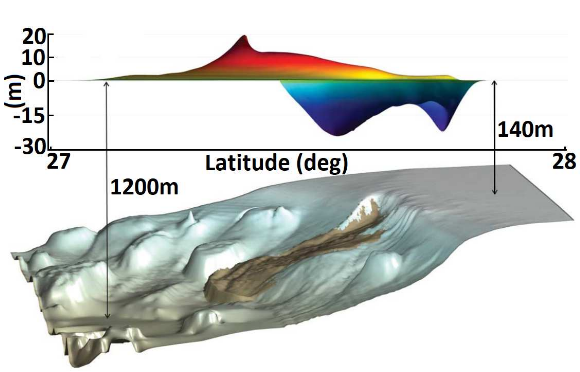

(d) TSUNAMI3D, 7 mins

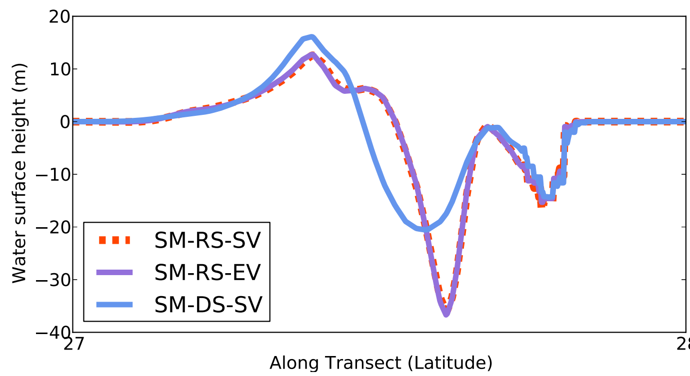

(e) Water elevation along transect through middle of the slide

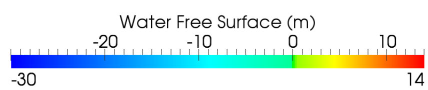

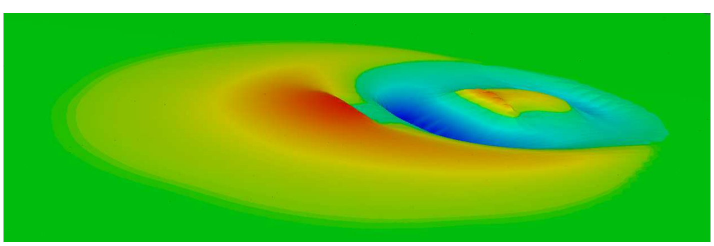

(f) SM-RS-EV, 10 mins

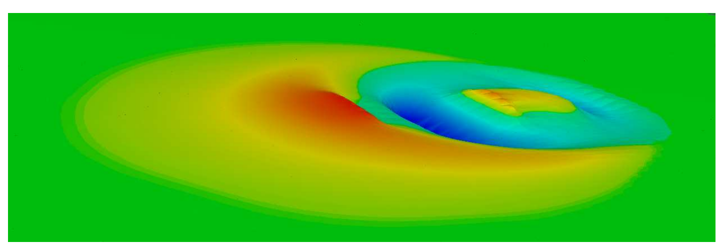

(g) SM-RS-SV, 10 mins

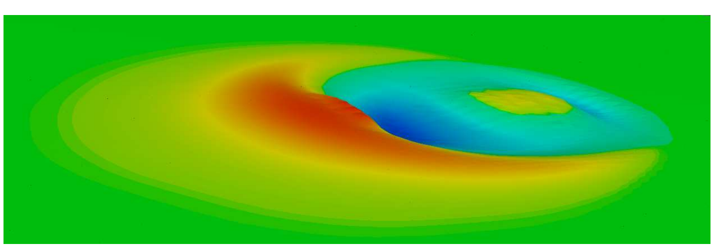

(h) SM-DS-SV, 10 mins

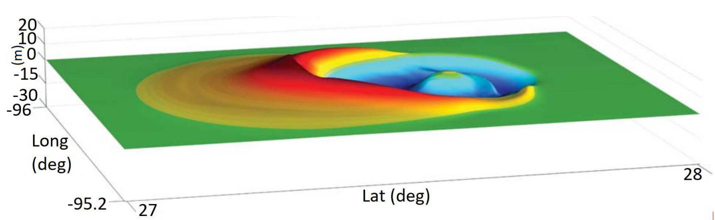

(i) TSUNAMI3D, 10 mins

Figure 3: Wave heights 7 minutes after slide initiation for (a) SM-RS-EV (b) SM-RS-SV (c) SM-DS-SV in the Gulf of Mexico test case. (d) shows results from Horrillo et al. (2013) for comparison. (e) shows the water elevation across the transect shown in Figure 1, this is the midpoint of the width of the slide. Colour plots shown span 27°– 28° N and 95.2°–96°W.

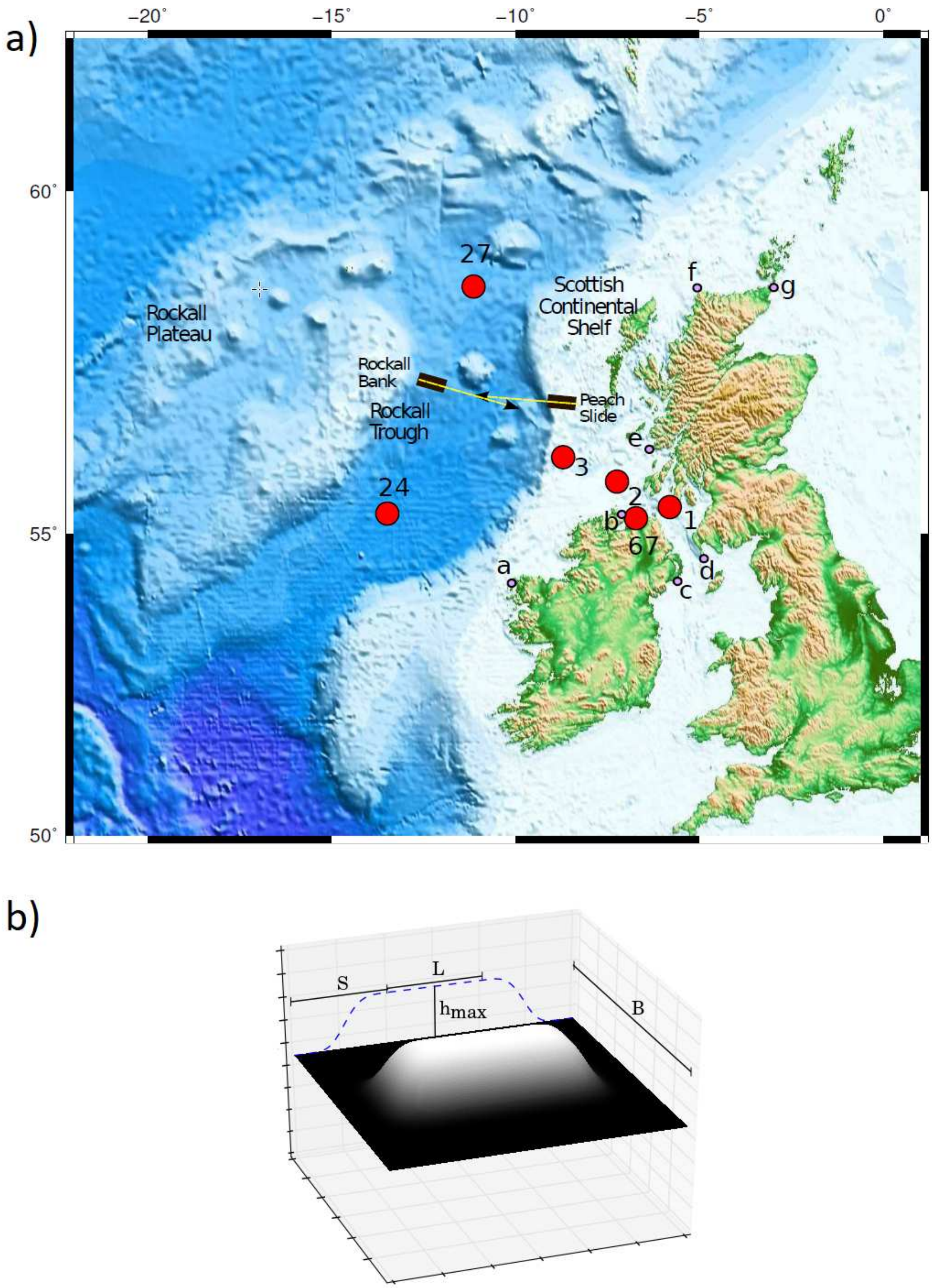

Figure 4: A) Map of British Isles with locations of Rockall Bank and Peach Slides, with arrows indicating directions of failure. Important bathymetric features are labelled. Red dots show locations of some of the numerical wave gauges to be considered later. B) Shape of rigid slide (exaggerated vertically) used in three dimensions, as described by Equation 11.

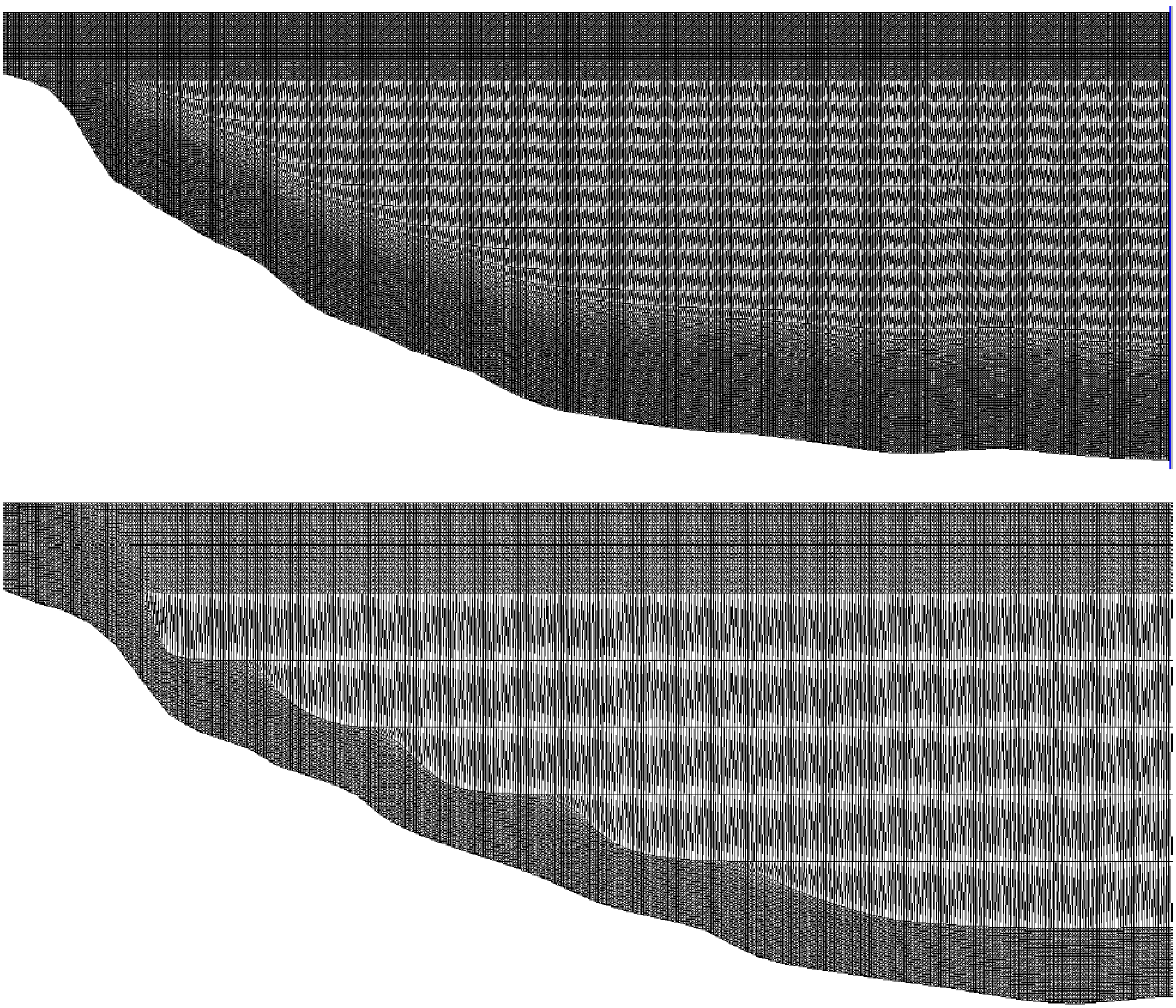

Figure 5: Section of Rockall Mesh (top) containing 2653 nodes and Peach Slide Mesh (bottom) containing 2984 nodes. There is a vertical exaggeration of x 10

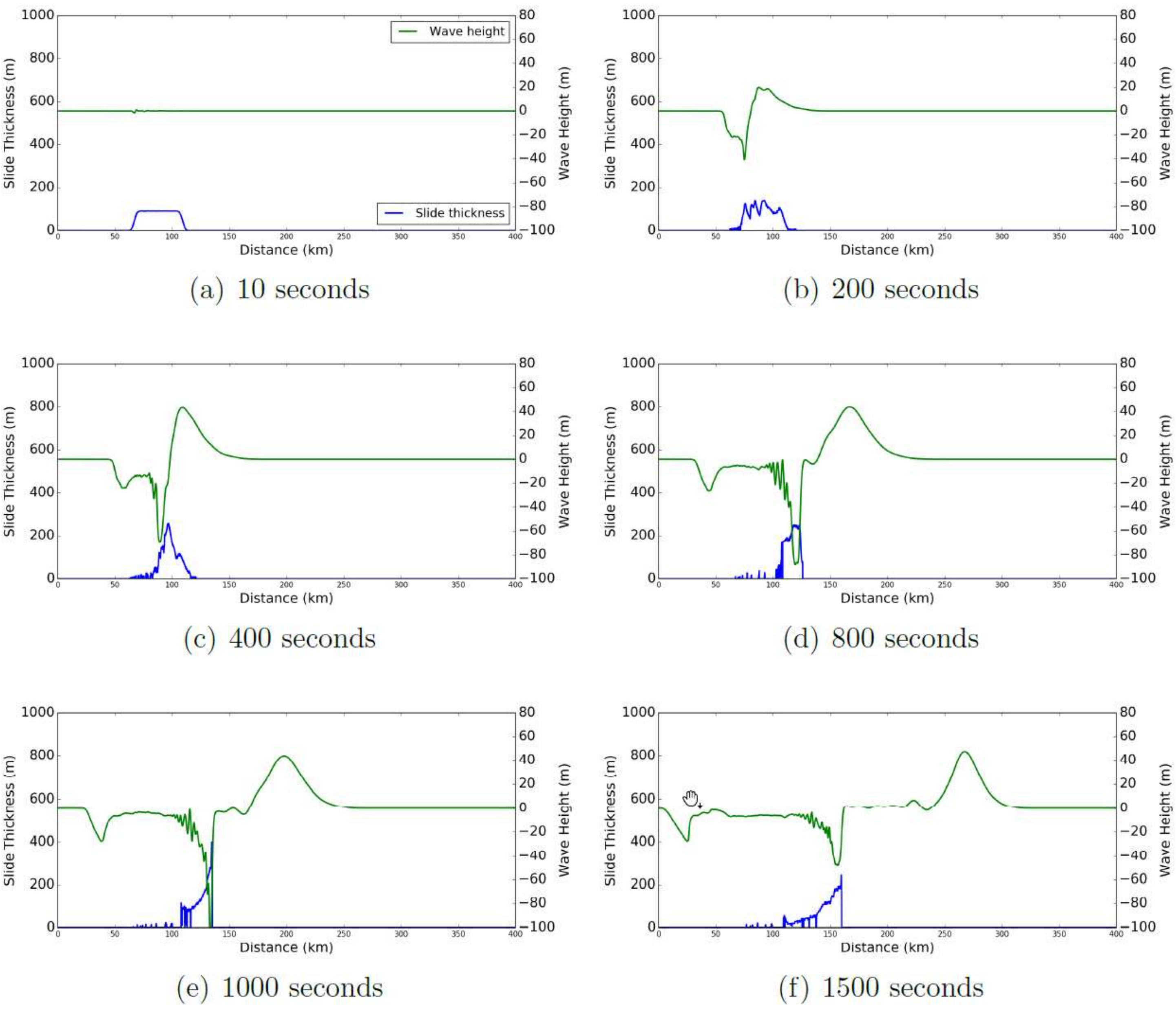

Figure 6: Slide thickness (blue) and wave height (green) for two-dimensional submarine slide at Rockall Bank, extracted from MM2FS simulation. Both are vertically exaggerated on different scales.

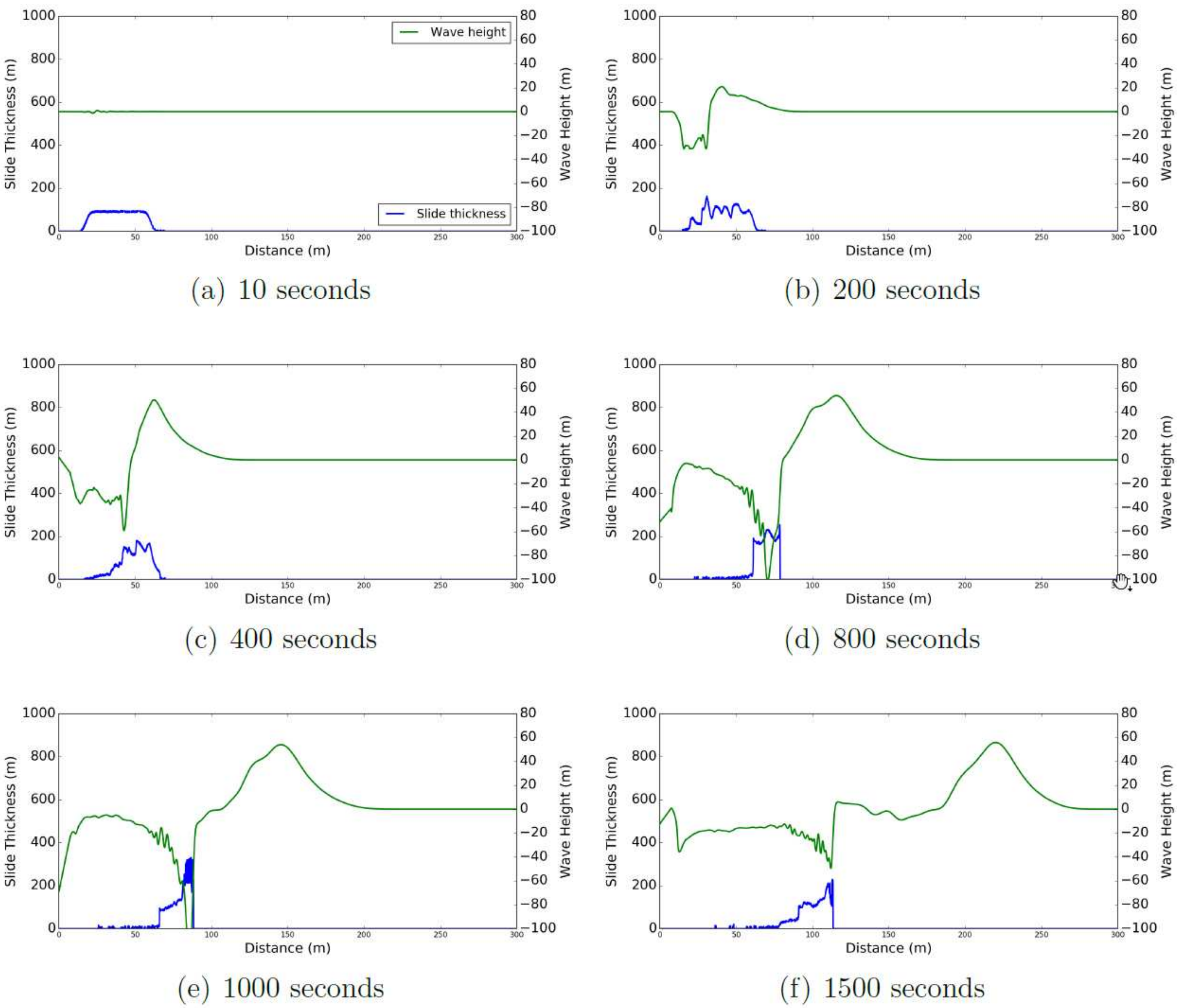

(a) 10 seconds (b) 200 seconds (c) 400 seconds (d) 800 seconds (e) 1000 seconds (f) 1500 seconds

Figure 7: Slide thickness (blue) and wave height (green) for two-dimensional submarine slide at Peach Slide, extracted from MM2FS simulation. Both are vertically exaggerated on different scales.

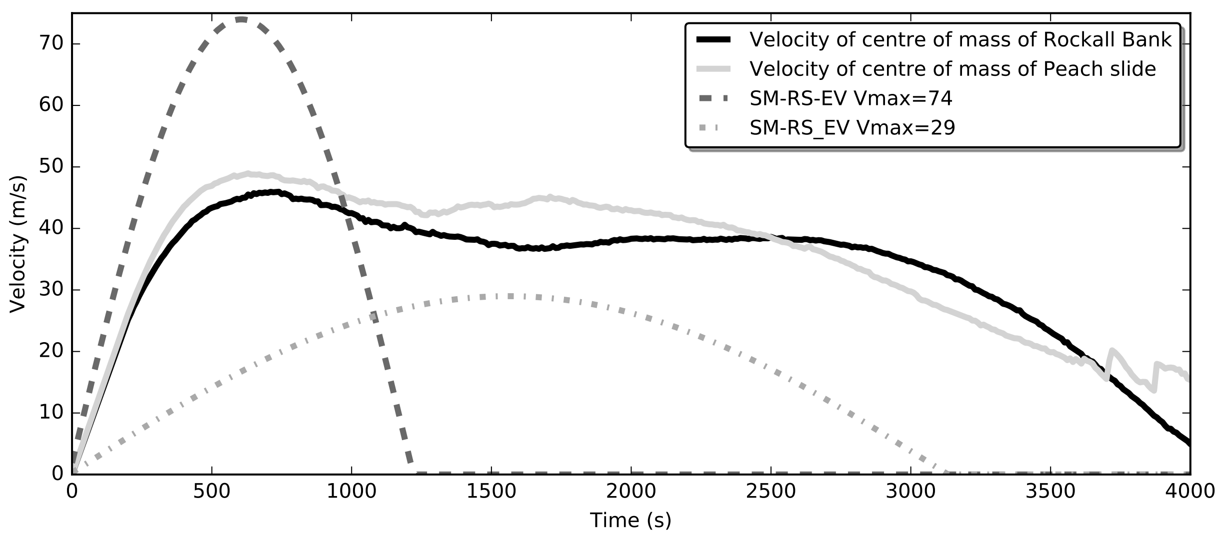

Figure 8: Velocity profiles representing the movement of the slide's centre of mass for Rockall Bank (solid black) and Peach slides (solid grey) and estimated slide velocity profiles for Rockall Bank scenarios with maximum velocities of 74m/s (dark grey, dashed) and 29 m/s (light grey, dot-dashed).

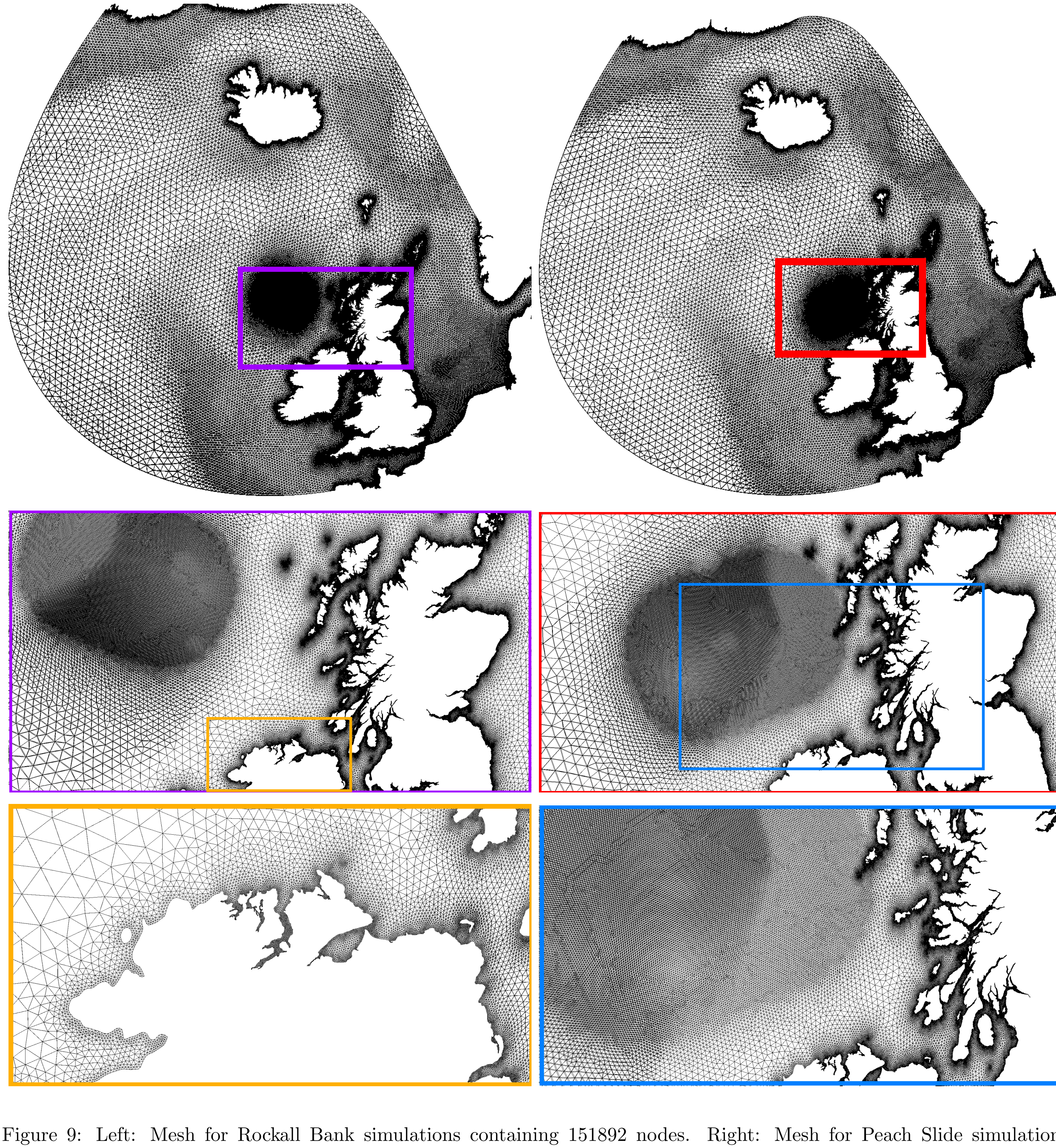

Figure 9: Left: Mesh for Rockall Bank simulations containing 151892 nodes. Right: Mesh for Peach Slide simulations containing 150257 nodes. The minimum edge length is 0.5 km and the maximum edge length is 50 km. The three dimensional domains have maximum extents at approximately 49°N, 70°N, 13°E, 30°W.

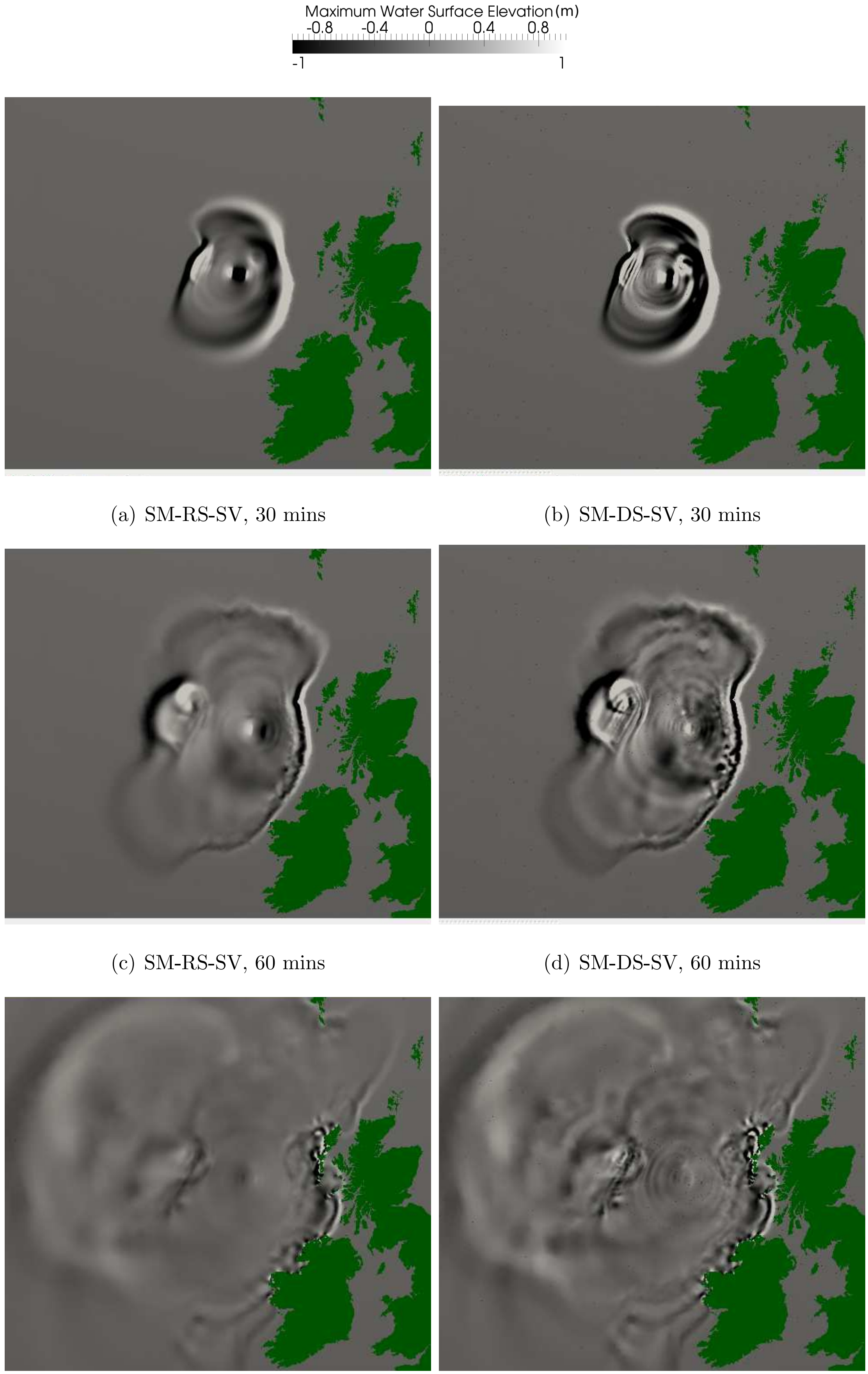

(a) SM-RS-SV, 30 mins

(b) SM-DS-SV, 30 mins

(c) SM-RS-SV, 60 mins

(d) SM-DS-SV, 60 mins

(e) SM-RS-SV, 110 mins

(f) SM-DS-SV, 120 mins

Figure 10: Wave height through time for Rockall Bank slide for the SM-RS-SV approach (left) and the SM-DS-SV approach (right). The scales for wave amplitude is capped at ± 1 m.

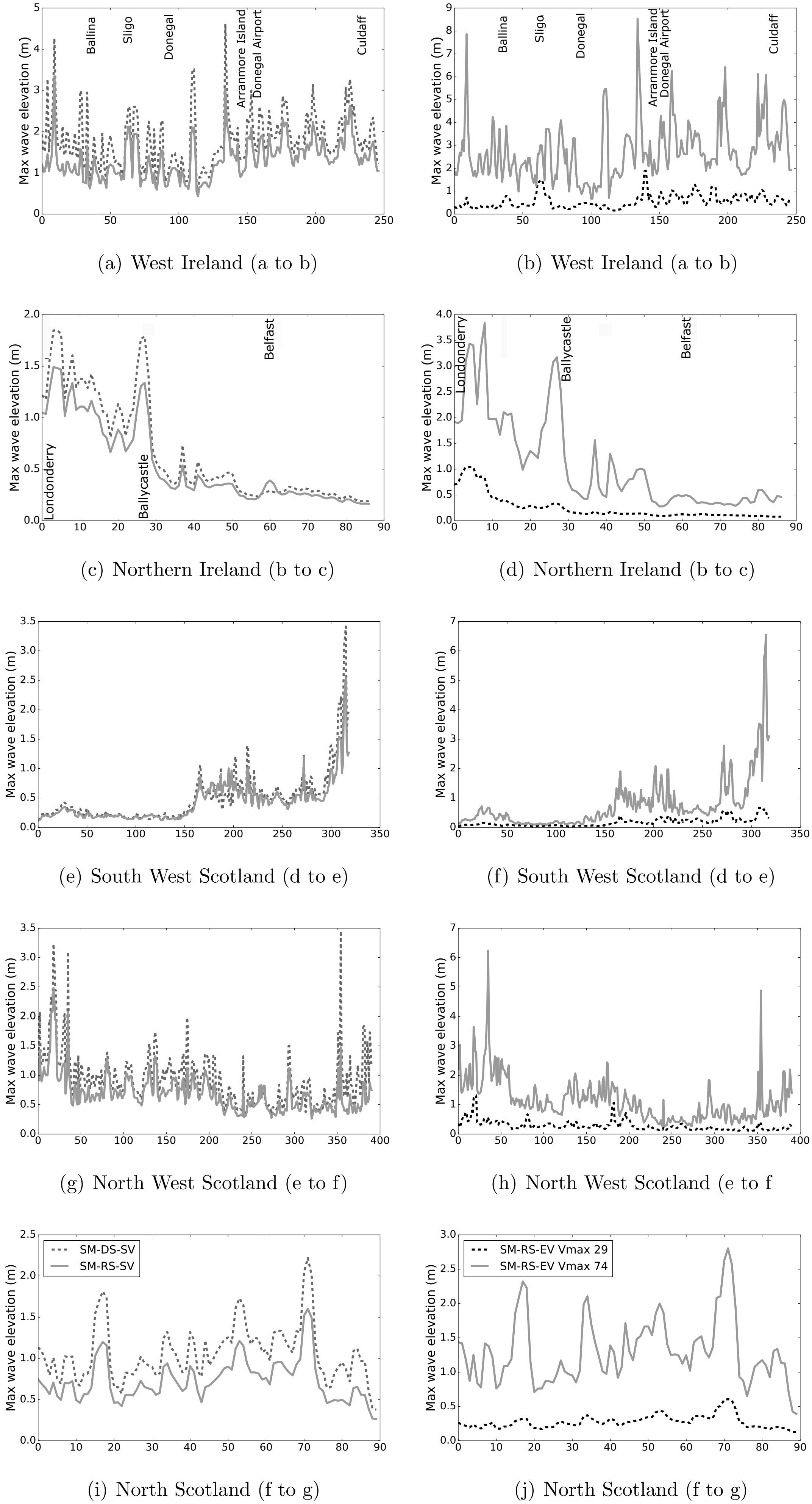

(a) West Ireland (a to b)
(b) West Ireland (a to b)
(c) Northern Ireland (b to c)
(d) Northern Ireland (b to c)
(e) South West Scotland (d to e)
(f) South West Scotland (d to e)
(g) North West Scotland (e to f)
(h) North West Scotland (e to f
(i) North Scotland (f to g)
(j) North Scotland (f to g)

Figure 11: Maximum water elevation at sections of coastline shown in Figure 4 for R1 vs R2 (left) and R3 vs R4 (right).

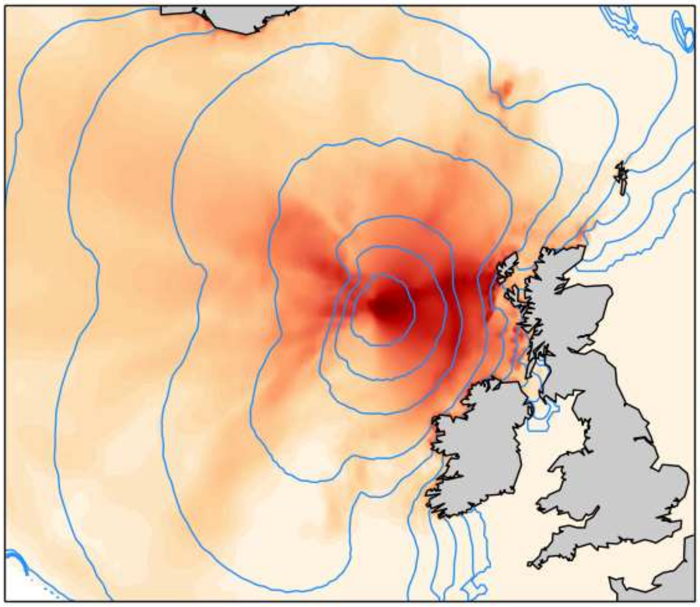

(a) Rockall Bank (SM-DS-SV)

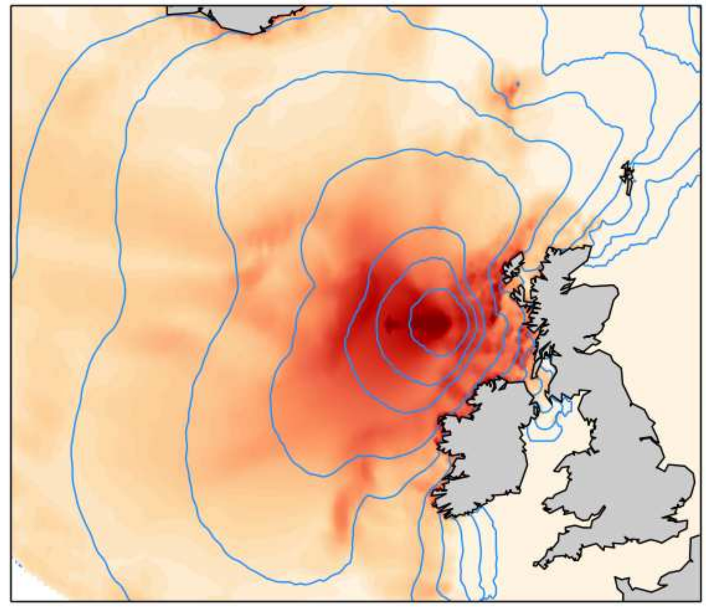

(b) Peach slide (SM-DS-SV)

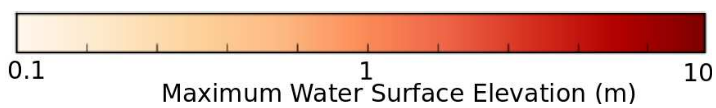

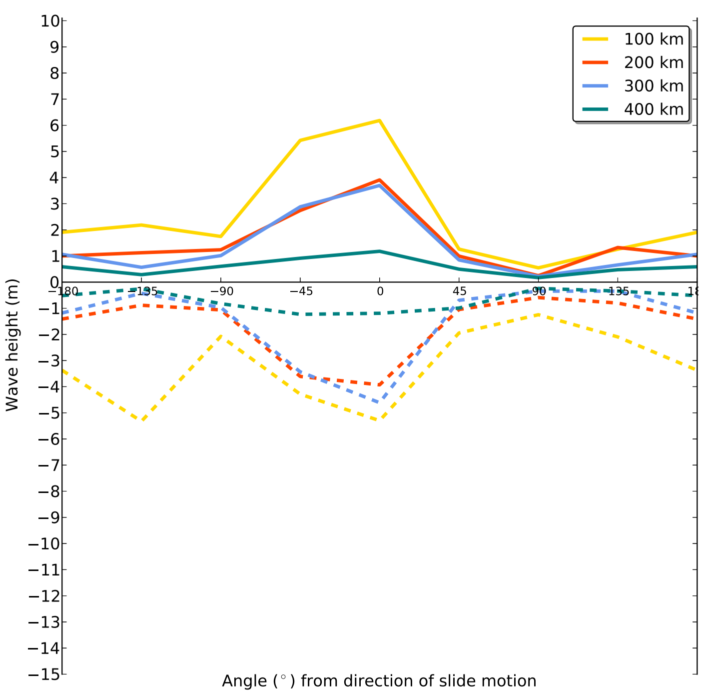

(c) Rockall Bank (SM-DS-SV)

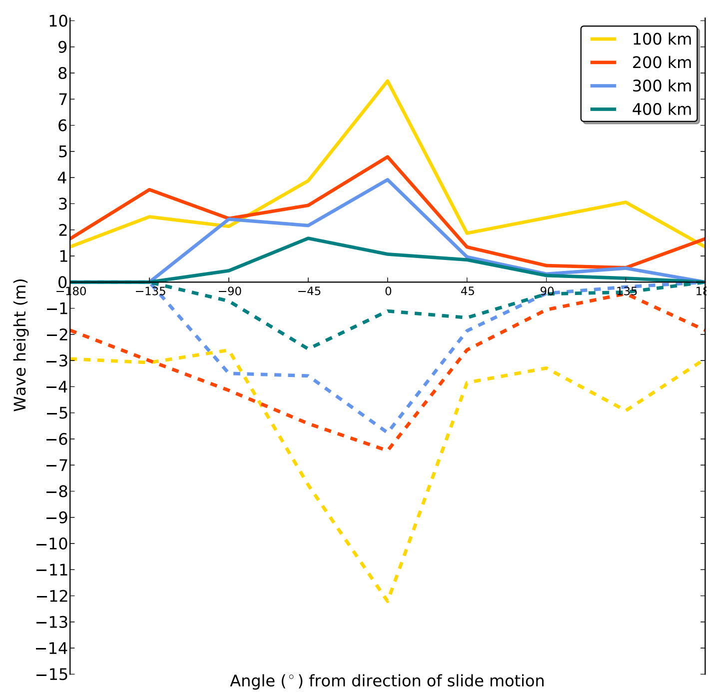

(d) Peach slide (SM-DS-SV)

Figure 12: Top: Maximum Water Elevation in first 4 hours and 15 mins after slide initiation for Rockall Bank Slide (left) and Peach slide (right) using SM-DS-SV approaches. Bottom: Maximum (solid lines) and minimum (dashed lines) wave heights recorded at numerical wave gauges 100 km (yellow), 200 km (red), 300 km (blue) and 400 km (green) from Rockall Bank (left) and Peach Slide (right) for SM-DS-SV.